

VEGETABLE MAPPING USING FUZZY DYNAMIC TIME WARPING

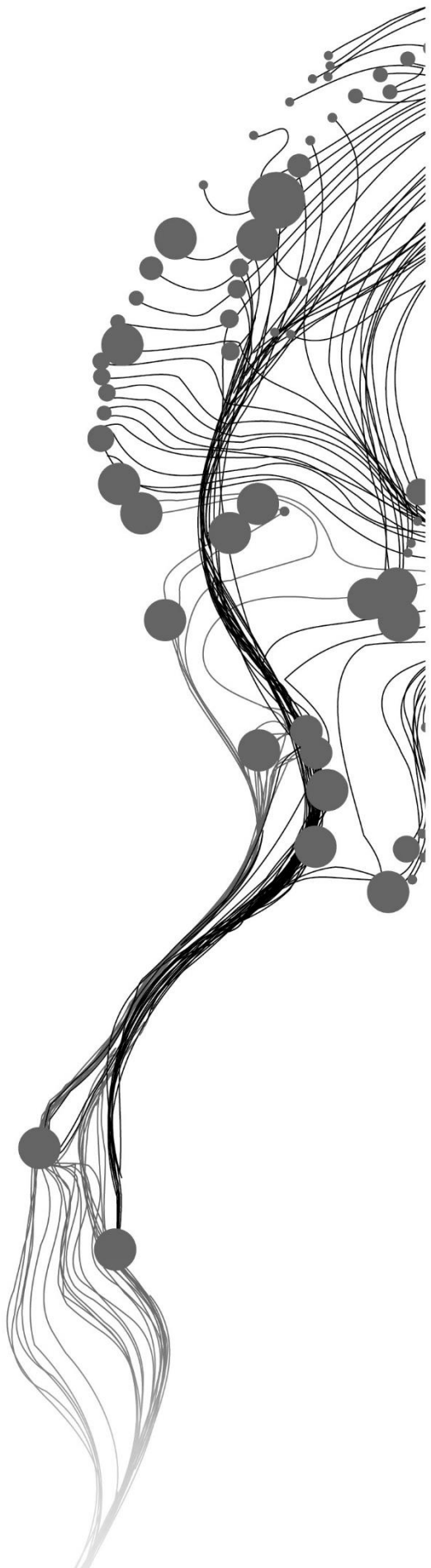
WISDOM SIMATAA MOOLA

July, 2020

SUPERVISORS:

dr.ir. W. Bijker

dr. M. Belgju



VEGETABLE MAPPING USING FUZZY DYNAMIC TIME WARPING

WISDOM SIMATAA MOOLA

Enschede, The Netherlands, June, 2020

Thesis submitted to the Faculty of Geo-Information Science and Earth Observation of the University of Twente in partial fulfilment of the requirements for the degree of Master of Science in Geo-information Science and Earth Observation.

Specialization: Geoinformatics (GFM)

SUPERVISORS:

dr. ir. W. Bijker

dr. M. Belgiu

THESIS ASSESSMENT BOARD:

prof.dr.ir. A. Stein (Chair)

dr. M. Li (External Examiner, Fuzhou University, China)

DISCLAIMER

This document describes work undertaken as part of a programme of study at the Faculty of Geo-Information Science and Earth Observation of the University of Twente. All views and opinions expressed therein remain the sole responsibility of the author, and do not necessarily represent those of the Faculty.

ABSTRACT

Fuzzy classification is an approach that is used in image classification when pixels are assigned membership to classes there are closely related. This research focuses on the concept of fuzzy classification to classify Time Weighed Dynamic Time Warping with Spring (TWDTWS) distances generated by TWDTWS algorithm on Sentinel 1A images. Determination of class separability was done using Transformed Divergency (TD) on the Vertically transmitted and Horizontally received (VH), Vertically transmitted and Vertically received (VV) and VH minus VV. The TWDTWS distances in each of the class queries for Chili, Tomato, Cucumber, Rice, Maize, Trees and Others were normalised. TWDTWS distances in each class query were first normalised and then used to compute fuzzy memberships for each class query using the Gaussian membership function. The computed fuzzy memberships for the best class and runner-up class in each pixel were then normalised to a sum of 1. Measure of similarity for Confusion Index (CI), Ambiguity Index (AI) fuzziness and fuzzy membership were used and different thresholds on each of the measures were applied in defuzzification. The result for TD shows that the classes are more separable when using the VH polarisation as compared to VV and VH minus VV. The results for accuracy assessment of the defuzzification output had an overall accuracy of 0.86 and kappa coefficient of 0.83 were obtained for thresholds of 0.6, 0.3, 1.2 and 0.7 for CI, AI, fuzziness and fuzzy membership respectively. The improved overall accuracy and kappa coefficient are due to pixels with less fuzzy memberships to the best class that remained unclassified. Therefore, further work should be undertaken using the approach used in this study when determining better sites for training and validation samples in remote sensing.

Keyword: Fuzzy membership, TWDTWS, Confusion Index, Ambiguity Index, Fuzziness

ACKNOWLEDGEMENTS

I would like to foremost express my gratitude to God Almighty for giving me good health, strength and inspiration in fulfilling my dream of studying at the Faculty of ITC of the University of Twente.

Secondly, I would like to thank NUFFIC for the OKP scholarship that gave me an opportunity to study at the University of Twente.

I would like to also thank my research supervisors, dr. ir. Wietske Bijker and dr. Mariana Belgiu for their guidance, patience and encouragement throughout the research phase.

I would like to thank Mengmeng Li, Sadhu Zukhruf Janottama and EWINDO field staff of the G4AW SMARTSeeds project for providing the field data used in this study.

I would like also to thank Sitanggang, Agmalaro, Hendrik and Li for developing the Python script I was able to use in data processing.

I would like to also thank my employer Zambia Forestry College under the Ministry of Lands and Natural Resources for allowing to pursue my studies by offering me the study leave.

I would like to thank the Philadelphia Seventh-Day Adventist Church members of Enschede for their spiritual and moral support during my stay in Enschede.

I would also like to thank my wife Deborah, my son, Humphrey, my parents, brothers and sister for their encouragements.

Finally, I would like to thank my friends like, Ferdinand Handavu, Field Hamalila, Katebe Sakala, Mulimba Yasini, Elly Mulenga, James Mulala, Euphravia, Moses, Misheck and Francina for their encouragement and motivation during my study period.

The list is endless, all in all I extend my gratitude to all who played a role that my academic progress can be a success.

TABLE OF CONTENTS

1.	INTRODUCTION.....	7
1.1.	Background and Motivation.....	7
1.2.	Research problem.....	8
1.3.	Conceptual Framework.....	10
2.	LITERATURE REVIEW.....	11
2.1.	SAR images.....	11
2.2.	SAR time-series images.....	11
2.3.	Dynamic Time Warping.....	12
2.4.	Fuzzy Classification.....	14
2.5.	Fuzzification.....	14
2.6.	Measures of Uncertainty.....	15
2.7.	Defuzzification.....	16
3.	METHODOLOGY.....	17
3.1.	Study area.....	17
3.2.	Research design.....	17
3.3.	Methodology.....	18
3.4.	Growth pattern.....	19
3.5.	Class separability.....	20
3.6.	TWDTWS distances.....	20
3.7.	Normalization of TWDTWS distances.....	20
3.8.	Measures of similarity and uncertainty.....	21
3.9.	Defuzzification.....	22
3.10.	Accuracy assessment.....	22
4.	RESULTS.....	23
4.1.	Growth patterns of the investigated crops.....	23
4.2.	Class separability.....	23
4.3.	TWDTWS distances.....	24
4.4.	Normalised fuzzy membership result.....	25
4.5.	Measures of similarity and uncertainty.....	26
4.6.	Defuzzification results.....	32
4.7.	Accuracy assessment.....	37
5.	DISCUSSION.....	39
5.1.	Class separability.....	39
5.2.	TWDTWS distances.....	39
5.3.	Spatial extent of CI, AI and fuzziness.....	40
5.4.	Defuzzification and validation.....	41
6.	CONCLUSION AND RECOMMENDATIONS.....	43
6.1.	Conclusion.....	43
6.2.	Recommendation.....	43
7.	Appendix.....	48

LIST OF FIGURES

Figure 1: Conceptual framework shows two types of classification, which are Hard and Soft classification. In hard classification, the classifier makes a decision in assigning a pixel to a crisp class while in soft classification, pixels are assigned fuzzy membership grades to several classes. Defuzzification is performed to make an easy understanding of the soft classification.	10
Figure 2: Illustration of the subsequence matching using the DTW distances with the black line indicating the optimal warping path (Sakurai et al., 2007). X is a data sequence of length n and Y is a query sequence of length m , x_i is the start of a qualifying subsequence of length l and ends at x_{i+l-1} . $x_1 \dots$ are semi-infinite sequence of numbers.....	14
Figure 3: Map showing the locations where field survey data was collected in Lampung, Indonesia, with the Google Earth image as the background.....	18
Figure 4 : Methodological flow chart showing the various steps involved in this study.....	19
Figure 5: Growth pattern for all classes with the subplot for the crop pattern with VH signal showing clear patterns of the start and the end of the crop season with the majority of classes separable. Subplot for the crop pattern with the VV signal and that of the VH-VV signal exhibit no clear crop growth pattern, and classes seem not to be separable easily.	23
Figure 6: Distribution of the TWDIEWS distances for each class query using Boxplots with mean and median represented inside each boxplot with a horizontal line and scatter point respectively. Each boxplot has a number a number of outliers. .25	25
Figure 7: Spatial distribution for fuzzy membership to the normalised best class. The extent of fuzzy membership to the best class ranges from 0.58 to 0.99.....	27
Figure 8: Spatial extents of the fuzzy membership for the normalised runner-up class. The extent of the fuzzy membership to the runner-up class ranges from 0.01 to 0.42.....	27
Figure 9: (a) Subset of the study site for the normalised fuzzy membership to the best class; (b) Subset of the Google Earth image corresponding to the subset of Figure 9(a). The areas with high fuzzy membership correspond to an agricultural crop field, while areas with trees and mixed land cover type have low fuzzy membership, as can be seen from a Google Earth image. Dark blue means low fuzzy membership values, while yellow is high membership values. The area is composed of both mountain areas with and flat terrain where agriculture is practiced.	28
Figure 10: CI map showing the spatial distribution of CI. If areas have low CI, it means that similarity between the best class and runner-up class is not close, but in areas were CI is high, it means that the best class and the runner-up class are similar hence high confusion at the pixel level.	29
Figure 11: AI map showing the spatial distribution of AI. Areas where the AI is low means that there is less uncertainty between the best possible class and the best achieved class while areas where the AI is high means there is high uncertainty as the difference between the best possible class and the achieved best class is large.	29
Figure 12: Fuzziness map showing the spatial distribution of the fuzziness for all the normalised fuzzy membership classes. High fuzziness means that those pixels have more fuzzy memberships closer to or equal to 0.5. If fuzziness is low, the pixels have fuzzy memberships closer to 1 and 0 for the best and runner-up class, respectively.	30
Figure 13: Subset of the study area the computation results for (a) Normalised fuzzy membership to the best class (b) Normalised fuzzy membership to the runner-up class (c) CI (d) AI. Pixels whose best class and runner-up class being similar have high CI while those that are not similar have low CI. Pixels with high values for the fuzzy membership to the best class have lower AI, while low values of best class results into high AI.	31
Figure 14: Subset of the study area showing the computational results for fuzziness. Pixels that have best class membership close to 1 and the runner-up class close to 0 have low fuzziness while those that have both membership classes closer to 0.5 have the highest values for fuzziness.	32
Figure 15: Crisp map generated from defuzzification of AI with a threshold of 0.3 where 51.74% pixels of the total image are classified.	33
Figure 16: Crisp map generated from defuzzification of CI with a threshold of 0.6 where 51.74% pixels of the total image classified.....	34

Figure 17: Crisp map generated from defuzzification of CI with a threshold of 0.7 where 95.64% pixels of the total image classified.	34
Figure 18: Crisp map generated from defuzzification of fuzziness with a threshold of 1.2 where 51.74% pixels of the total image classified.	35
Figure 19: Crisp map generated from defuzzification of fuzziness with a threshold of 1.4, where 95.64% pixels of the total image classified.	35
Figure 20: Crisp map generated from defuzzification of fuzzy membership with a threshold of 0.7, where 51.74% pixels of the total image classified.	36
Figure 21: Google Earth image subsets of the field study sites. (A) Chili (B) Tomato (C) Cucumber (D) Rice (E) Maize (F) Trees and Others. It can be seen that the field study sample for Trees class has different cover classes.	36
Figure 22: User's accuracy of the defuzzification outputs for AI, CI, fuzziness and fuzzy membership to the best class. $AI \leq 0.3$, $CI \leq 0.6$, $Fuzz_1 = 1.2$ and $\mu \geq 0.7$ have higher and similar User's accuracy compared to $CI \leq 0.7$ and $Fuzz_1 = 1.4$	38
Figure 23: Producer's accuracy of the defuzzification outputs for AI, CI, fuzziness and fuzzy membership to the best class where $CI \leq 0.7$ and $Fuzz_1 = 1.4$ have higher and similar Producer's accuracy compared to $AI \leq 0.3$, $CI \leq 0.6$, $Fuzz_1 = 1.2$ and $\mu \geq 0.7$	38

LIST OF TABLES

<i>Table 1: Metadata of the Sentinel-1 images used in this study.....</i>	<i>17</i>
<i>Table 2: Class separability results for VH polarisation using the TD with all classes indicating that they are separable. ...</i>	<i>24</i>
<i>Table 3: Class separability for VV polarisation using the TD measure</i>	<i>24</i>
<i>Table 4: Class separability for VH minus VV using the TD measure.....</i>	<i>24</i>
<i>Table 5 : Descriptive statistics of the minimum TWD/TWS distances.....</i>	<i>25</i>
<i>Table 6: Percentage of the total number of pixels classified based on the defuzzification threshold applied.</i>	<i>33</i>
<i>Table 7: Overall accuracy and Kappa coefficient of the defuzzification output for AI, CI, fuzziness, and fuzzy membership to the best class.</i>	<i>37</i>
<i>Table 8: Error matrix for a crisp map of CI with a threshold of 0.6.</i>	<i>48</i>
<i>Table 9: Error matrix for a crisp map of CI with a threshold of 0.7.</i>	<i>48</i>
<i>Table 10: Error matrix for a crisp map of AI with a threshold of 0.3.....</i>	<i>48</i>
<i>Table 11: Error matrix for a crisp map of fuzziness with a threshold of 1.2.....</i>	<i>49</i>
<i>Table 12: Error matrix for a crisp map of fuzziness with a threshold of 1.4.....</i>	<i>49</i>
<i>Table 13: Error matrix for a crisp map of normalised fuzzy membership for best class with a threshold of 0.7.</i>	<i>49</i>

1. INTRODUCTION

1.1. Background and Motivation

Vegetable production plays an important role at the local and national level in terms of socio-economic, food and nutritional security for people in urban and rural areas of developing countries (Joosten, Dijkxhoorn, Sertse and Ruben, 2015). The increase in population has created market demand from customers seeking to diversify their diets with vegetables (Schreinemachers, Simmons, & Wopereis, 2018). This increase in demand for vegetables provides a greater potential for economic growth among smallholder farmers. This increase in population and demand for vegetables requires city planners and policymakers to have useful decision tools such as maps. Maps can help in making projections for future agriculture land with per capita vegetable consumption that maximizes local food production. Maximized food production results in improved food security, nutrition, and other social benefits that come with the involvement of locals in agriculture (Hara, McPhearson, Sampei, & McGrath, 2018).

The monitoring of crops and vegetables can be done generally with the use of optical images obtained from satellites (Stendardi et al., 2019). However, optical imagery has limitations during acquisition under cloud cover conditions as it affects the quality of details in the image for further analysis (Stendardi et al., 2019). It is for this reason that Synthetic Aperture Radar images (SAR) offer an alternative solution to the effects of cloud cover as they are less affected by the atmosphere and clouds because they operate in the microwave range, which can pass with less attenuation (Stendardi et al., 2019). Dusseux, Corpetti, Hubert-Moy, & Corgne (2014) stated that SAR data can be used to map different vegetables grown over different seasons as the images are not affected by cloud cover. Just like optical images, SAR images have the capability of frequent measurements of crops over short growing seasons because SAR sensors provide time series in the medium and high resolution of C band data (Stendardi et al., 2019).

SAR images have different polarization combinations that are based on the transmission and reception of backscattered signals from the target. These polarisation combinations are HH (horizontal transmit and horizontal receive), VV (vertical transmit and vertical receive), HV (horizontal transmit and vertical receive), and VH (vertical transmit and horizontal receive) (Najafi, Hasanlou, & Akbari, 2019). Based on these polarisation combinations, various scattering mechanisms can be extracted, which include surface, double bounce, and volumetric scattering. The obtained polarization combinations result in different images that have different applications. For example, Li et al. (2019) stated that VV polarization is suitable for separation of land cover types, while VH is suitable for separation of maize crop from low-growing crops. This study revealed that VH outperformed the VV polarisation in terms of the reported classification results. It is for this reason that SAR classification results can be of benefit to Agribusiness and Non-Governmental Organisations (NGOs) who are running projects in communities aimed at improving people's livelihoods. For example, SMARTSeeds Project is one of the projects that aims to enhance the quality of service delivery

on farmer support to farmers through input delivery and on-farm training in vegetable management practices to local communities of Indonesia. SMARTSeeds aims at improving people's livelihoods, food security, and nutrition. Currently, the SMARTSeeds project has the aim of supporting 100 000 (target not yet met) vegetable farmers to be self-reliant through increased production, income, and food security (SMARTSeeds, 2019).

1.1.1. Related studies

Dynamic Time Warping (DTW) is an algorithm that is used for measuring the similarity of time-series events when there is a minor distortion through the matching of the reference sequence and a test sequence (Ibrahim & Valli, 2015). In remote sensing, DTW can perform classifications based on time series and able is able to overcome the problem of irregular temporal gaps caused by cloudy images as is the case of optical images (Viana, Girão, & Rocha, 2019). Switonski, Josinski, and Wojciechowski (2018) stated that DTW is an elastic measure type in which a section of one sequence is mapped to another sequence that is relatively larger. In some situations, DTW can be applied in the classification of motion-captured data where time instants of compared sequences are matched in a nonlinear, monotonic transformation (Switonski et al., 2018). In short, motion data can also be applied in any study focussing on temporal changes such as vegetable mapping.

New versions of DTW have been formulated to enhance the performance of time series matching. One of them is the Time-Weighted Dynamic Time Warping (TWDTW) (Maus et al., 2016). TWDTW was formulated by introducing a time weighing constraint to the original DTW so as to overcome the temporal restriction that allows for phase shift resulting from seasonal changes of natural and cultivated vegetation (Maus et al., 2016). The TWDTW algorithm was formulated to capture seasonality changes in natural and cultivated crops growing over different seasons and later to map them accurately from time-series images.

In a recent study, Li & Bijker (2019) made some refinement to the TWDTW by incorporating the SPRING strategy to it and called it Time-Weighted Dynamic Time Warping with SPRING strategy (TWDTWS). In their study, the TWDTWS was used to classify vegetables of Chili, Tomato, and Cucumber from Sentinel 1A time-series images. The findings from their research revealed that TWDTWS has the potential of providing means of distinguishing vegetable types from Sentinel 1A time-series images with few redundancies as compared to just using TWDTW.

1.2. Research problem

TWDTWS algorithm is a hard classifier because the classifier defines the query sequences and calculates the dissimilarity cost and directly applies it in the classification without taking into account conditional class probabilities in estimating the class membership for chili, tomato, and cucumbers (Li & Bijker, 2019). They reported that the overall accuracy of the TWDTWS classification for the Malang dataset was 0.80, with a

kappa coefficient of 0.77. For the Lampung dataset, the overall accuracy was 0.87, and the kappa coefficient was 0.82. Though these classification accuracies are reasonable, the study does not provide information about how close the runners up classes are from the best classification result of the class. This measure is vital as it gives confidence in the classification results. Information of the runners up classes in remote sensing is essential as it can be used to measure similarity and certainty between the best class and runners up classes (Hofmann, 2016). In order to measure similarity and certainty, the concept of fuzzy sets could be applied in the classification process. The main idea of fuzzy sets is that each pixel is assigned to class memberships of between zero to one (0-1) (Onashoga, Ojesanmi, Johnson, & Ayo, 2018). Onashoga et al. (2018) further stated that a membership function can be used to define how each element is mapped to a membership grade. In remote sensing membership grades are used for computing measures of similarity and certainty between the best class and the runners class in each pixel.

Therefore, this study aims at using the TWDTWS distances to compute class memberships using a Gaussian membership function. The generated class memberships will then be used to identify areas with high uncertainty as a means of improving the remote sensing image classification using fuzzy memberships generated from minimum TWDTWS distances. The findings in this study will help in input and service delivery to vegetable farmers who will also benefit from the timely receiving of inputs and training in vegetable management, leading to high income, food security and nutrition.

1.2.1. Research Objectives

The research objective of this study is to create a fuzzy version of the TWDTWS classifier and use it to characterise uncertainties among classes spatially in a vegetable map.

Specific objective

1. Identify a fuzzy membership function to use in fuzzification.
2. Determine the spatial extent of the measure of similarity and certainty for each class.
3. Evaluate the performance of the Fuzzy Dynamic Time Warping algorithm.

Research question

- a. How can minimum TWDTWS distance be applied in the generation of fuzzy membership grades?
- b. What is the appropriate fuzzy membership function to be applied in defining fuzzy membership values?
- c. How can TWDTWS distances be used to express uncertainty in a map?
- d. How can the measures of uncertainty be used to improve remote sensing classification accuracy?

1.3. Conceptual Framework

In remote sensing classification, there are two approaches followed, namely hard and soft classification. In the case of soft classification, each pixel is assigned a measure of degree of similarity (membership) to every class of the classification scheme (Choodarathnakara, Ashok Kumar, Koliwad, & Patil, 2012). In contrast, during hard classification, class probability estimation is used to decide on classification boundary in the feature space so that each pixel is assigned to one class (Liu, Zhang, & Wu, 2011). Figure 1 shows the conceptual framework that has been used in this study. The main concepts are SAR images, Hard classification, and Soft classification. In hard classification, the TWDTWS classifier generates TWDTWS distances that are used to label classes by comparing a temporal signature of a known query to unknown time series (or sequence) (Maus et al., 2016). In the case of soft classification, the TWDTWS classifier is used to generate TWDTWS distances, of which membership to classes are produced using the Gaussian membership function where pixels belonging to a class have varying memberships. The final step in soft classification is defuzzification in which fuzzy membership grades are turned to crisp values for a better understanding of the classification outputs (Onashoga et al., 2018).

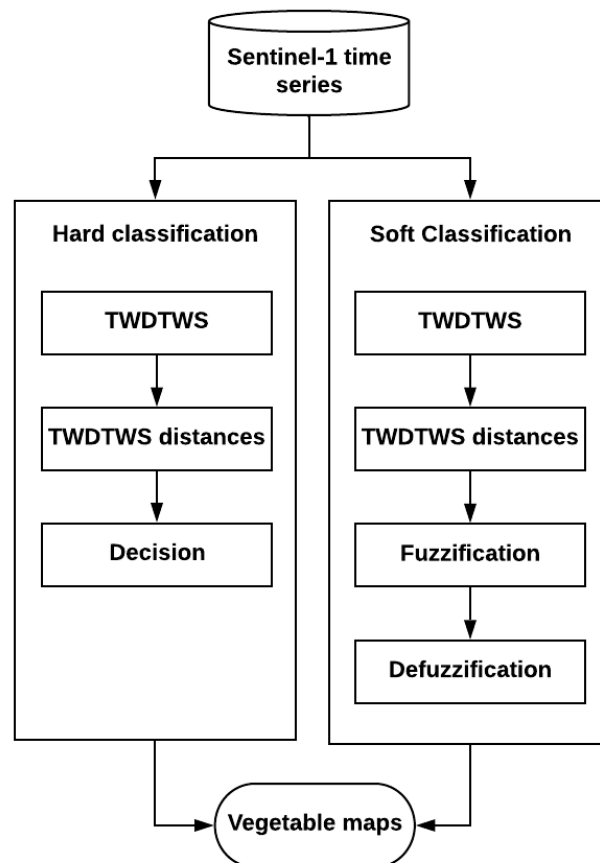


Figure 1: Conceptual framework shows two types of classification, which are Hard and Soft classification. In hard classification, the classifier makes a decision in assigning a pixel to a crisp class while in soft classification, pixels are assigned fuzzy membership grades to several classes. Defuzzification is performed to make an easy understanding of the soft classification.

2. LITERATURE REVIEW

2.1. SAR images

In remote sensing, SAR images are captured using Radar sensors that utilize the microwave wavelength. Radar sensors have an advantage over the optical remote sensing in agriculture applications as they are not affected by the atmosphere and clouds (Stendardi et al., 2019). The main reason is that Radar sensors operate in different wavelength bands that have the ranges of 0.75cm to 107cm, including K band (0.75cm to 2.40cm), X band (2.40cm to 3.75cm), C band (3.75cm to 7.50cm), S band (7.5cm to 15cm), L band (15cm to 30cm) and P band (30cm to 107cm) (Skolnik, 1990). Furthermore, Thenkabail (2015) stated that the Sentinel-1A sensor operates in C band with a wavelength range of 3.75cm to 7.50cm. Sentinel-1A images have four different polarizations, which are HH, VV, HV, and VH. These polarisations have different applications in radar remote sensing. The reason is that different polarizations of SAR images are useful for land use and land cover discrimination. It is possible to discriminate land cover because different features in an image have different polarimetric responses (Dusseux et al., 2014). The other advantages of SAR images are that the Radar sensors have a short repeat cycle of 12 days (Onojeghuo et al., 2018) and are also not affected by cloud cover in areas where cloud coverage is very high during summer (Dusseux et al., 2014) such as the tropics. This short repeat cycle means that valuable information about crop growth status can be obtained and used for monitoring of crops to achieve sound agriculture management and policy-making (Chang-an et al., 2019).

Different studies have revealed that Sentinel-1A can be used to map crops. For instance, Li et al. (2019), in their research, used Sentinel-1A to precisely identify Maize to determine the accurate planting area and yield times. Jiang et al. (2019) reported that SAR images could be used to study the phenological evolution of each crop cultivated in a field as each growing plant produces a unique temporal profile of the backscatter coefficient. This temporal profile about the crop phenology serves as the critical information that can be used to differentiate different crops. Sentinel-1A images are used in crop mapping because the SAR backscatter signal is sensitive to crop and field conditions such as growth stages, biomass development, plant morphology, soil moisture and irrigation conditions (Jiang et al., 2019). The use of SAR backscatter over the growing season has been used as key information in delineating rice areas (Mosleh, Hassan, & Chowdhury, 2015).

2.2. SAR time-series images

Time-series images of SAR are critical in remote sensing as they provide valuable information that can be used in extracting biological phenomena on the earth's surface. For instance, Stendardi et al. (2019) stated that a dense time series images are necessary for understanding SAR signal behaviour about crops as a means of extracting phenological features. For example, grassland identification can be performed better with time

series as compared to single date image due to different spectral responses resulting from different management practices applied during the growing season (Dusseux et al., 2014).

In recent years, times series similarity has been gaining numerous prospects in remote sensing applications such as the extraction of vegetation areas whose output data has many uses (Guan, Huang, Liu, Meng, & Liu, 2016). For instance, SAR images are gaining numerous prospects because they are readily available to users and also have less restriction in terms of acquisition time as can be acquired during day or night time. In agriculture, it is possible to obtain crop growth dynamic information from time-series images (Chang-an et al., 2019). The data collected can be used as a reference in future planning of what crops to plant and the spatial location of the fields. SMARTSeeds project in Indonesia, uses spatial data to contact farmers and advise them on best vegetable management practices to attain food security and income generation at the household level (SMARTSeeds, 2019).

2.3. Dynamic Time Warping

DTW originated from dynamic programming algorithm and it was applied in speech recognition (Sakoe & Chiba, 1978). Sakoe & Chiba (1978) used dynamic programming algorithm in pattern matching of spoken word with a nonlinear time normalisation effect. They modelled time-axis fluctuation with a nonlinear warping function so that the timing differences between two speech patterns is eliminated so that maximum coincidence is achieved. It is from this background that the DTW algorithm was developed to match and calculate distances between two time series or sequences. DTW is a distance measurement method that has been used widely in measuring similarity in time series (different sequences) when there are minor distortions in the time axis (Ibrahim & Valli, 2015). The DTW algorithm is one of the distance measures used for time series data that is not limited to one mapping but also supports non-equal-length time series (Niennattrakul & Ratanamahatana, 2007). For this reason, the DTW algorithm is said to be an effective classifier for time series classification and clustering because of its non-linear mapping capabilities (Jeong, Jeong, & Omitaomu, 2011). The algorithm aims at finding an optimal match between two sequences by allowing non-linear mapping of one sequence to another and minimize the distance between the two sequences (Jeong et al., 2011). Upon completion of the distance computation, the two sequences are then warped in a non-linear manner to determine their similarity independent of any variations in the time dimensions (Ibrahim & Valli, 2015). In this case, the optimal match is the one that corresponds to the lowest distance path after aligning the two sequences one onto another as illustrated in Figure 2. The DTW algorithm computes distances for all points between the two sequences of the reference point and testing point (Jeong et al., 2011). Dynamic programming technique is also applied when finding the minimal distance between the two time-series where the sequences are warped by stretching or shrinking the time dimension (Guan et al., 2018).

In recent years, important improvements have been made to the DTW algorithm as a way of enhancing its effectiveness in time-series classification. Maus et al. (2016), for example, improved the original DTW by

introducing a temporal constraint so that the temporal range is put into perspective when finding the best alignment between two time series. The modification was done with a view of enhancing shape matching that takes into account seasonality changes of landcover types when applied to remote sensing. The temporal constraint that was introduced to the DTW is the time weighed and the algorithm was named Time-Weighted Dynamic Time Warping (TWDTW). The TWDTW algorithm is said to be suitable for classification of remote sensing time series where the temporal variation is more important than the spatial variations (Maus et al., 2016).

Further modification to the TWDTW has been performed as mentioned in the paper Li & Bijker (2019). The improvement to the TWDTW was aimed at increasing the computational speed and subsequence searching. In their research, they improved the TWDTW algorithm by incorporating a SPRING algorithm that can detect qualifying subsequences correctly at an enhanced speed (Sakurai, Faloutsos, & Yamamuro, 2007). Li & Bijker (2019) named this new version of TWDTW as Time Weighed Dynamic Time Warping with SPRING strategy (TWDTWS). The advantage of the TWDTWS to the original TWDTW is that its computationally more efficient as compared to the TWDTW.

2.3.1. SPRING strategy

SPRING is a streaming algorithm used for sub-sequence matching in the data streams (Sakurai et al., 2007). This algorithm is capable of detecting efficiently high similarity subsequences in a data stream. Sakurai et al. (2007) stated that the SPRING algorithm can address the problem that involves a data stream X which is discrete with semi-infinite numbers $x_1, x_2, \dots, x_n, \dots$, where x_n is the most recent value and n increases with every new time-tick. They used $X[t_s : t_e]$ to denote the subsequence that starts from t_s and ends at t_e . The algorithm can be used when there is a need of finding a subsequence $X[t_s : t_e]$ that has high similarity to a fixed-length query sequence Y i.e smallest DTW distance. The other use is that of the issue when the sequence X has a fixed length n and Y of length m and there is a need of finding subsequence in the $X[t_s : t_e]$ whose DTW distance from Y is the smallest among a number of all possible subsequences $X[t_s : j]$ that are heavily overlapping. In the case of overlapping matches only the local minimum DTW distance of the overlapping subsequences is reported. The most prominent advantage of the SPRING is that its drastically fast, and the algorithm can identify the qualifying subsequences in a stream fashion. It is for this reason that the SPRING was incorporated to the TWDTW to have TWDTWS for subsequence searching and speed computations in vegetable classification using time series of SAR images (Li & Bijker, 2019).

distribution of the Gaussian function (Siler & Buckley, 2004). The Gaussian membership function assumes that the classes are normally distributed with an infinity support base (Siler & Buckley, 2004; Kumar, Saravana, Rout, Pandit, & Snehmani, 2012).

In fuzzification, each entity becomes a gradual member of the fuzzy classification. This means that pixels will be assigned gradual memberships to classes based on the classification scheme. Therefore, a pixel is composed of the best membership class and the runner-up class memberships (Hofmann, 2016).

In remote sensing, the total sum of fuzzy membership for each pixel should sum up to unity (1) because the membership degrees inside a pixel closely match landcover proportions (Bezdek, Ehrlich, & Full, 1984; Matsakis, Andréfouët, & Capolsini, 2000). However, it is not always a must that the total sum of membership for a pixel should equal to 1 as in the case of fuzzy membership derived from artificial neural network (Foody, 1996).

2.6. Measures of Uncertainty

In fuzzy classification, some measures can be applied to a fuzzy membership degree of a class to measure the uncertainty in the classification. These measures of uncertainty include the Confusion Index (CI), Ambiguity Index (AI), and Fuzziness.

CI is a measure that measures how fuzzy membership differs between the best class and the runners up classes and the range for CI is from 0 to 1. Higher values of CI closer to 1 mean that the runner up class has membership grade similar to the best class, i.e., high uncertainty. Lower values of CI closer to zero indicate that the runners up class and the best class are not similar hence the uncertainty is also low (Hofmann, 2016). The formula for CI is shown in Equation 1 adopted from Burrough, Van Gaans, & Hootsmans (1997)

$$CI = 1 - (\mu_0 - \mu_i) \quad (1)$$

where μ_0 is the membership for the best class result and μ_i is membership for the runners up class.

The second measure of uncertainty is AI, which is the measure of uncertainty between the best possible membership grade and the best-achieved membership of a pixel. In this case, the best possible membership for a pixel is 1. The range for AI is from 0 to 1 and a value for AI = 0 indicates that there is less uncertainty in the fuzzy classification, while AI = 1 means that there is high uncertainty (Hofmann, 2016). The formula for AI is shown in equation 2 as adopted from Hofmann (2016)

$$AI = 1 - \mu_0 \quad (2)$$

The third measure of uncertainty is fuzziness which is defined as the measure of extent to which a fuzzy set is not a crisp set (Siler & Buckley, 2004). Fuzziness tends to be higher when there are more memberships of 0.5 in a pixel and thereby make the classification to be fuzzier. For example if a pixel has two similar memberships belonging to the best class and runner class of 0.5 each, its fuzziness will be 2 (Siler & Buckley, 2004). Similarly, fuzziness decreases when there are more class memberships of 0 or 1 (Hofmann, 2016). Fuzziness can be computed using equation 3 as adopted from Siler & Buckley (2004)

$$Fuzz_1 = \sum_{i=0} (1 - |2\mu_i - 1|) \quad (3)$$

where $Fuzz_1$ is fuzziness.

2.7. Defuzzification

Defuzzification is a process by which elements in a fuzzy set are converted to a crisp value deemed to be the best representative of the fuzzy set (Klir & Yuan, 1995). The defuzzification process is performed to achieve a better understanding of the output of the fuzzy classification (Onashoga et al., 2018). Matsakis et al. (2000) state that during defuzzification, pixels have to be assigned to a class to which they have the highest membership.

2.7.1. Decision Rules for Defuzzification

During defuzzification, the user sets up decision rules to guide the process in terms of how pixels are to be assigned to crisp sets. CI, AI and fuzziness thresholds can be used to decide which pixels are to be classified and others unclassified. When a threshold value has been decided by the user for AI, CI and fuzziness, all pixels whose values are found to be below the thresholds are defuzzified and assigned to a class it has the highest membership (Islam & Metternicht, 2005). On the other hand, the pixels with values above the selected thresholds for AI, CI and fuzziness remain unclassified (Hofmann, 2016).

3. METHODOLOGY

3.1. Study area

The study area for this research is Lampung of the Island of Sumatra, Indonesia. The study area location coordinates are 5° 2' 42" S, 104° 42' 0" E and 5° 24' 43.2" S, 105° 24' 0" E. The study area was chosen because there is an ongoing project for SMARTSeeds that is closely working with farmers to improve their livelihoods through vegetable growing (SMARTSeeds, 2019).

The region of Lampung has a tropical climate with a relative humidity of 60 to 80%, temperatures of 23 °C to 37 °C, and annual precipitation ranging from 2257 to 2454 mm/year (Banuwa et al., 2019). Dewi, Sasmito, Aziz, Parwito, & Sari (2019) mentioned that Indonesia experiences two seasons throughout the year, which are the dry and wet season. Higher precipitation in this area occurs from December to April. The landscape of Lampung is relatively flat (Li & Bijker, 2019).

3.2. Research design

3.2.1. Data source

Python Scripts

Python scripts for the automated data processing used in this study were developed based on the SARauto Python scripts developed within the G4AW SMARTSeeds project by Sitanggang, Agmalaro, Hendrik, & Li (2019) based on earlier MATLAB scripts developed by Li as described in Li & Bijker (2019).

SAR images

In this study, Sentinel-1A time-series satellite images from 1st April to 28th October 2018 were downloaded from Copernicus Open source Hub: <https://scihub.copernicus.eu/dhus/#/home>. Sentinel-1A images were chosen as they are not affected by clouds and atmosphere and have a short repeat cycle of 12 days (Stendardi et al., 2019). Table 1 shows the summary metadata for the images

Table 1: Metadata of the Sentinel-1 images used in this study

Data	Satellite platform	Product type	Sensor mode	Swath	Range resolution	Azimuth resolution	Date
Sentinel-1A	S1A	Ground Range Detected (GRD)	Interferometric Wide Swath (IW)	250km	5m	20m	2018

Reference data

Field survey data used in this study was collected by Mengmeng Li, Sadhu Zukhruf Janottama and EWINDO field staff in July 2018 as part of the G4AW SMARTSeeds project. A total number of 66 field site samples located within the study area composed of Chili, Tomato, Cucumber, Rice, Maize, Trees and Others. From these field survey samples, 29 training and 34 validation sub-samples independent from each other were used. Their location is shown in Figure 3.

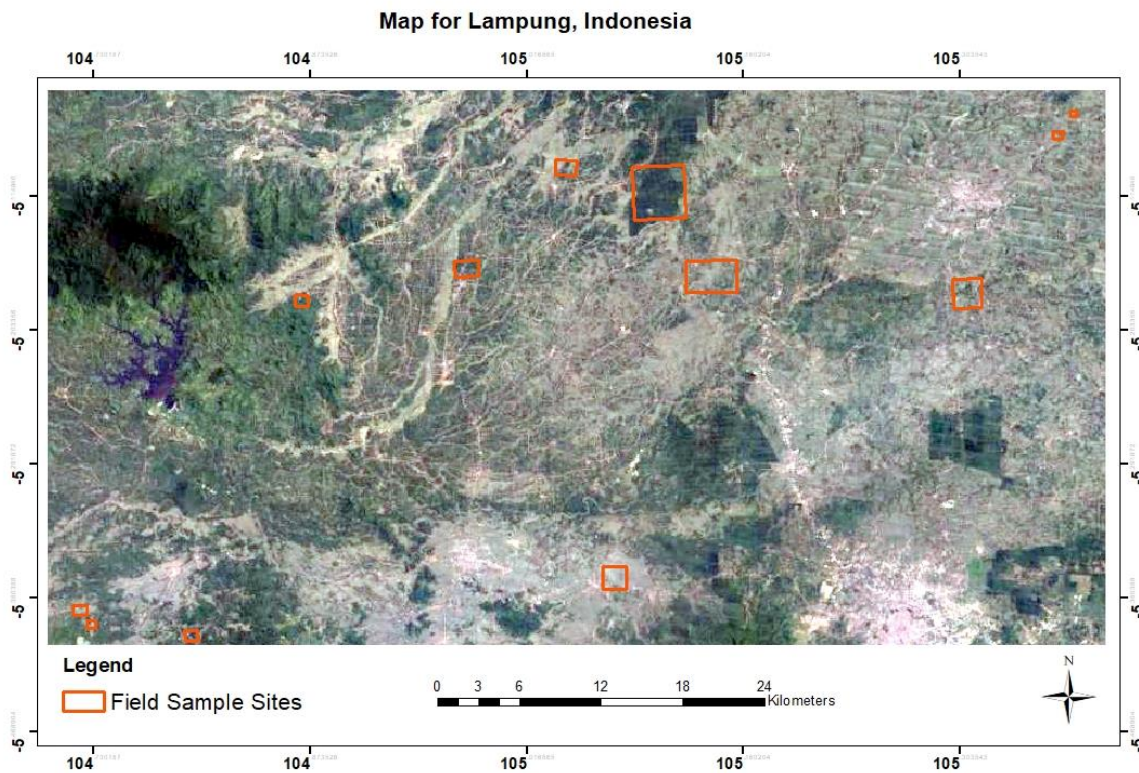


Figure 3: Map showing the locations where field survey data was collected in Lampung, Indonesia, with the Google Earth image as the background.

3.3. Methodology

3.3.1. Image processing

The methods applied in this research are presented in Figure 4. The main input are Sentinel-1A time-series images. The images were processed using the European Space Agency (ESA) toolbox, the Sentinel Application Platform (SNAP) version 7.0 (SNAP, 2019). SNAP implementation is there to extract the VV and VH from the dual polarised backscattered time series (Jiang et al., 2019). An automated image processing workflow developed by Sitanggang et al. (2019) as described in Li & Bijker (2019), was applied in this research. The processing started with the downloading of the images, Apply the Orbit Profile, Radiometric calibration, Speckle filtering and Terrain correction.

After downloading the images, the orbit profile was applied by SNAP to download the latest released orbit profile so as to get a precisely geocoded product. Radiometric calibration was then applied in order to convert digital numbers for pixels to a radiometrically calibrated backscatter directly related to the radar backscatter of the scene. Polarimetric Speckle filtering was done using the SNAP integrated Refined Lee filter with a window size of 7 x 7. This filter aims at reducing speckle noise while preserving spatial resolution, polarimetric scattering property and statistical characteristics of the backscatter signal (Lee, Fellow, Ainsworth, Wang, & Chen, 2015).

Other steps implemented in the methodological flow chart include the execution of the TWDTWS algorithm. The purpose of TWDTWS is to perform pattern matching of the backscatter polarisation in the time series to the training dataset. Fuzzification of the minimum TWDTW distances was performed, followed by the defuzzification and accuracy assessment of the fuzzy classification.

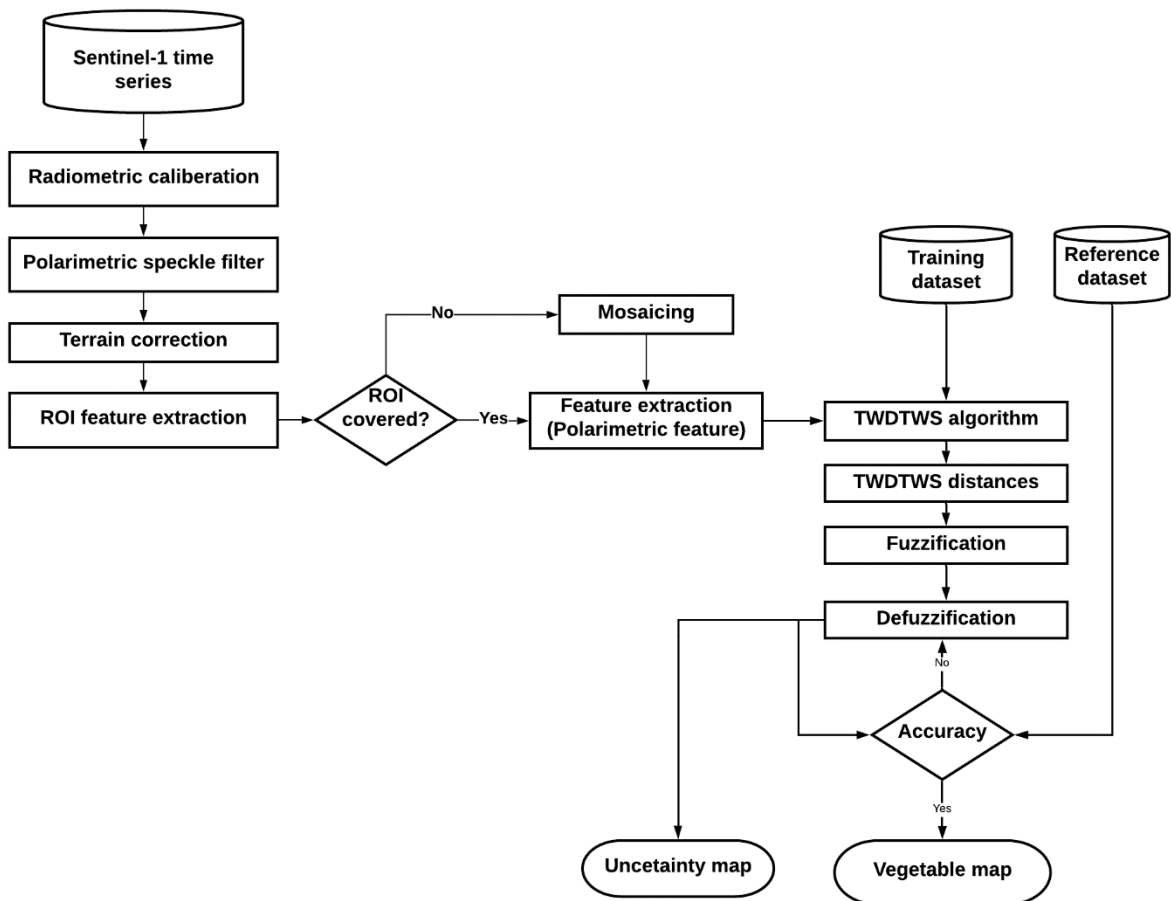


Figure 4 : Methodological flow chart showing the various steps involved in this study.

3.4. Growth pattern

Growth patterns for the crops Chili, Tomato, Cucumber, Rice, Maize, Trees and Others were generated from a total of 476 pixels collected from the training samples. Class query sequences were created based on the VH, VV and VH minus VV polarisation. Mean for each date of the samples for each class was obtained.

Savitsky-Golay filter was applied to smoothen and fit the data points for the polarisation features to a polynomial in a least-squares sense (Savitzky & Golay, 1964). Growth patterns were generated in order to determine the polarisation where class separability is possible.

3.5. Class separability

Measure of class separability using the VH, VV and VH minus VV polarisation was conducted using the Transformed Divergence (TD). This was done to determine the feature in which classes are separable based of the training data for the TWDTWS algorithm. The formula to compute TD is shown in equation 4 and 5 (Swain & Davis, 1978).

$$D_{ij} = \frac{1}{2} \text{tr}[(V_i - V_j)(V_i^{-1} - V_j^{-1})] + \frac{1}{2} \text{tr}[(V_i^{-1} - V_j^{-1})(M_i - M_j)((M_i - M_j)^T)] \quad (4)$$

$$TD = 2000 \left[1 - \exp\left(\frac{-D_{ij}}{8}\right) \right] \quad (5)$$

where D_{ij} is divergence between i and j signature classes compared, $V_i - V_j$ are the covariance matrix of signature i and j, $M_i - M_j$ are the mean vector for signatures i and j, tr is the trace function (matrix algebra), T is the transposition function and TD is Transformed Divergence.

3.6. TWDTWS distances

TWDTWS algorithm proposed by Li & Bijker (2019) was applied to generate TWDTWS distances for the classes of Chili, Tomato, Cucumber, Rice, Maize, Trees, and also a class named as Others.

3.7. Normalization of TWDTWS distances

Query subsequence for all target classes were generated from the TWDTWS classification. The normalization of TWDTWS distances for each pixel in each class query was computed using the total sum of TWDTWS distances in a class. The aim for normalization of TWDTWS distances was to have a total sum of the normalized TWDTWS distances equal to 1, as suggested by Bezdek, James C., Robert Ehrlich, & William Full(1984). The normalization process of the TWDTWS distances was performed using equation 6

$$x_i = \frac{TWDTWS_i}{\sum TWDTWS_i} \quad (6)$$

where x_i is the normalized TWDTWS distance and $TWDTWS_i$ represent the minimum TWDTWS distance for a pixel belonging to a class.

3.7.1. Fuzzification

The Gaussian membership function was used to compute fuzzy memberships from the normalized TWD/TWS distances. The Gaussian membership function was used because it follows a standard normal distribution curve with a gradual change in membership values that does not reach a zero value. The Gaussian membership function applied as adopted from Kumar et al. (2012) is shown in equation 7

$$\hat{\mu}_i = \exp\left(-\frac{(x_i - \bar{x}_c)^2}{2\sigma_c^2}\right) \quad (7)$$

where $\hat{\mu}_i$ is the membership function(or membership grade) of the Gaussian membership function, x_i is the normalised TWD/TW distance of class query sequence, \bar{x}_c and σ_c stands for the mean and standard deviation of the normalised TWD/TW distances to the class query sequences, respectively.

The sum for fuzzy memberships that are generated by the Gaussian membership function for each pixel does not equal to 1. Therefore, normalisation of the best class and runner-up class membership for each pixel has to be done in order for the sum of all memberships in a pixel equal to 1. Equation 8 was used to normalise the fuzzy memberships

$$\mu_i = \frac{\hat{\mu}_i}{\sum_i \hat{\mu}_i} \quad (8)$$

where μ_i is normalised fuzzy membership, $\hat{\mu}_i$ is the original fuzzy membership in a pixel. Note that all the measures of similarity will use the normalised fuzzy memberships to the best and runner-up classes.

3.8. Measures of similarity and uncertainty

3.8.1. Confusion Index

The measure of similarity between the best class and the runner-up classes in a class query was performed using the CI based on the normalised fuzzy memberships. CI was used to express the ambiguity of an entity's fuzzy classification (Hofmann, 2016). Equation 1 was used to compute CI.

3.8.2. Ambiguity Index

AI was computed based on the normalised achieved best class membership and the best possible fuzzy membership. The best possible fuzzy membership to a class is 1. AI was computed based on equation 2.

3.8.3. Fuzziness

Fuzziness was used to compute the extent at which the fuzzy membership fails to have crisp memberships, i.e., either 0 or 1 (Siler & Buckley, 2004). Equation 3 was used for the computation of fuzziness.

3.9. Defuzzification

Defuzzification of the fuzzy classification of the TWD/TWS distances was done based on AI, CI, fuzziness and the normalised fuzzy membership to the best class. Different threshold values were based on the range for AI, CI, fuzziness and fuzzy membership. The chosen threshold values of AI, CI and fuzzy membership for defuzzification were 0.1, 0.2, 0.3, 0.4, 0.5, 0.6, 0.7, 0.8 and 0.9. In the case of fuzziness the thresholds chosen are 0.2, 0.4, 0.6, 0.8, 1.0, 1.2, 1.4, 1.6 and 1.8. The range of threshold for fuzziness is different from those of AI, CI and fuzzy membership as fuzziness is dependent on the number fuzzy membership classes considered and in this study, only the best class and the runner-up classes were considered. This means that fuzziness will increase based on the number of fuzzy memberships of 0.5 for the best and runner-up classes (Siler & Buckley, 2004). The threshold values were chosen in order to address the uncertainty in the classification. These values were chosen in order to find an effective threshold that would give a better overall accuracy result.

3.10. Accuracy assessment

The reference dataset used in this study was from the field data collected for the SMARTSeeds project in July, 2018. Separate independent sub-samples from the training samples were generated for validation of the classification. A total number of 633 points independent from the training set were randomly picked from the ground reference dataset. This set of points were used for the evaluation of the defuzzification output on thresholds that had a reasonable number of classified pixels. The Error matrix was made for the output of the defuzzification for AI, CI, fuzziness and fuzzy membership for thresholds that result into many pixels unclassified. The chosen threshold with many unclassified should also result into reasonable number of classified pixels. For each error matrix user accuracy, producer accuracy, overall accuracy and kappa's coefficient were computed (Congalton, 1991).

4. RESULTS

4.1. Growth patterns of the investigated crops

The results depicted in Figure 4 show the growth pattern of the crops for Chili, Tomato, Cucumber, Rice, Maize Trees, and Others using the VH, VV, and VH minus VV signals, respectively is plotted against the Date of Year (DOY). The curves show that VH signal help separate Chili, Tomato, Cucumber, Rice, Maize, and Other crops from each other. In the curves for VV and VH minus VV does not a better growth pattern as compared to the on with VH.

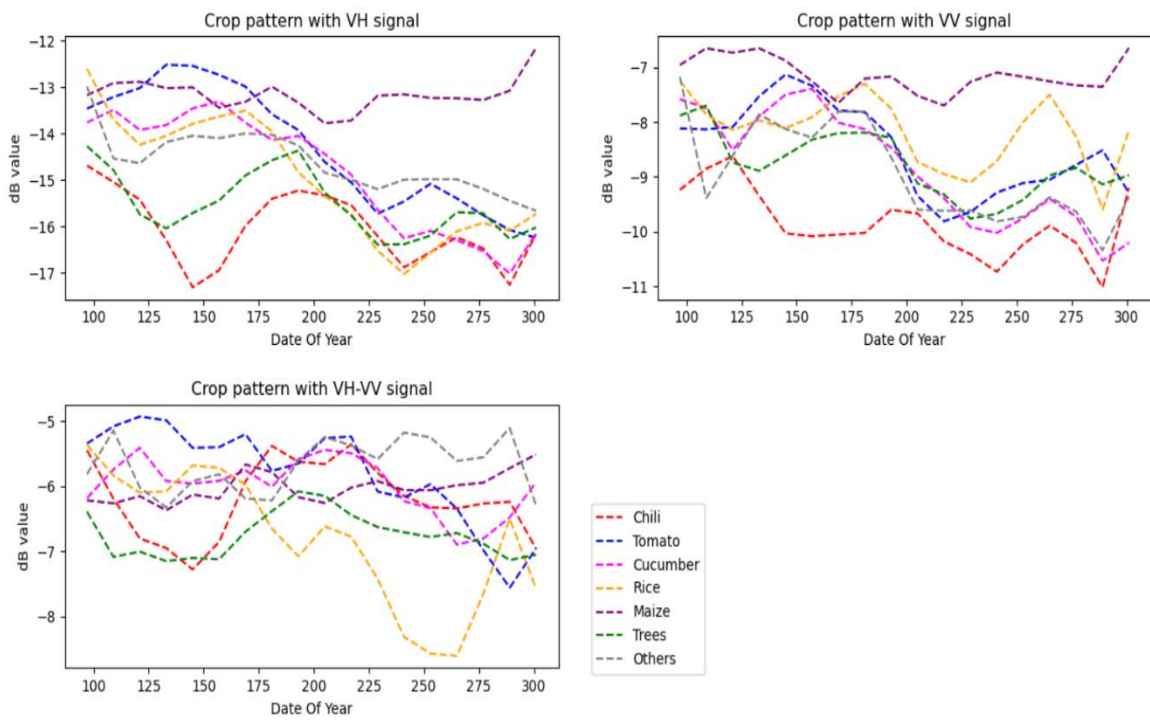


Figure 5: Growth pattern for all classes with the subplot for the crop pattern with VH signal showing clear patterns of the start and the end of the crop season with the majority of classes separable. Subplot for the crop pattern with the VV signal and that of the VH-VV signal exhibit no clear crop growth pattern, and classes seem not to be separable easily.

4.2. Class separability

Tables 2 to 4 shows the results for class separability using TD from the VH, VV and VH minus VV polarisations, respectively. The results emphasize that using the class pairs for Chili-Tomato, Chili-Cucumber, Chili-Rice, Tomato-Cucumber, Tomato-Rice, Cucumber-Rice, Tomato-Trees, Cucumber-Trees and Rice-Trees have the highest values of 2000 using the VH polarisation as shown in Table 2. In this polarisation, the least TD of 1713 was recorded between the Maize-Others class pair.

In the case of VV polarisation, the TD values for the class pair are all lower than the ones using the VH (Table 3). Similar results are obtained using VH minus VV, as can be seen in Table 4.

Table 2: Class separability results for VH polarisation using the TD with all classes indicating that they are separable.

Class	Tomato	Cucumber	Rice	Maize	Trees	Others
Chili	2000	2000	2000	1923	1999	1999
Tomato		2000	2000	1999	2000	1999
Cucumber			2000	1998	2000	1999
Rice				1999	2000	1997
Maize					1850	1713
Trees						1943

Table 3: Class separability for VV polarisation using the TD measure

Class	Tomato	Cucumber	Rice	Maize	Trees	Others
Chili	1960	1996	1885	812	1821	1980
Tomato		1940	1907	980	1696	1943
Cucumber			1962	1395	1766	1985
Rice				837	1414	1821
Maize					762	1235
Trees						1879

Table 4: Class separability for VH minus VV using the TD measure

Class	Tomato	Cucumber	Rice	Maize	Trees	Others
Chili	1486	1005	1876	537	392	755
Tomato		1194	1923	686	768	1055
Cucumber			1696	427	422	623
Rice				1243	1223	1558
Maize					206	306
Trees						319

4.3. TWDTWS distances

The TWDTWS distances generated from the TWDTWS classification show that the TWDTWS distances are normally distributed but slightly negatively skewed (slightly skewed to the right), as presented in Table 2. This means that the mean is slightly smaller than the median of TWDTWS distance in a class query. Of all the classes, the one with the highest skewness is the one for the Others class then followed by cucumber class, and the class with the least skewness is the one for trees class. The distribution of the TWDTWS distances is shown in Figure 6.

Table 5 : Descriptive statistics of the minimum TWDTWS distances

Class	Chili	Tomato	Cucumber	Rice	Maize	Trees	Others
Minima of minimum TWDTWS distances	0.270	0.264	0.270	0.239	0.275	0.258	0.247
Maxima of minimum TWDTWS	0.521	0.508	0.505	0.495	0.481	0.503	0.500
Mean of minimum TWDTWS distances	0.392	0.392	0.397	0.379	0.387	0.381	0.384
Variance of minimum TWDTWS distances	0.0005	0.0005	0.0005	0.0006	0.0005	0.0006	0.0006
Standard dev. of minimum TWDTWS distances	0.023	0.022	0.022	0.025	0.023	0.024	0.025
Skewness of minimum TWDTWS distances	-0.096	-0.085	-0.177	-0.13	-0.132	-0.033	-0.301

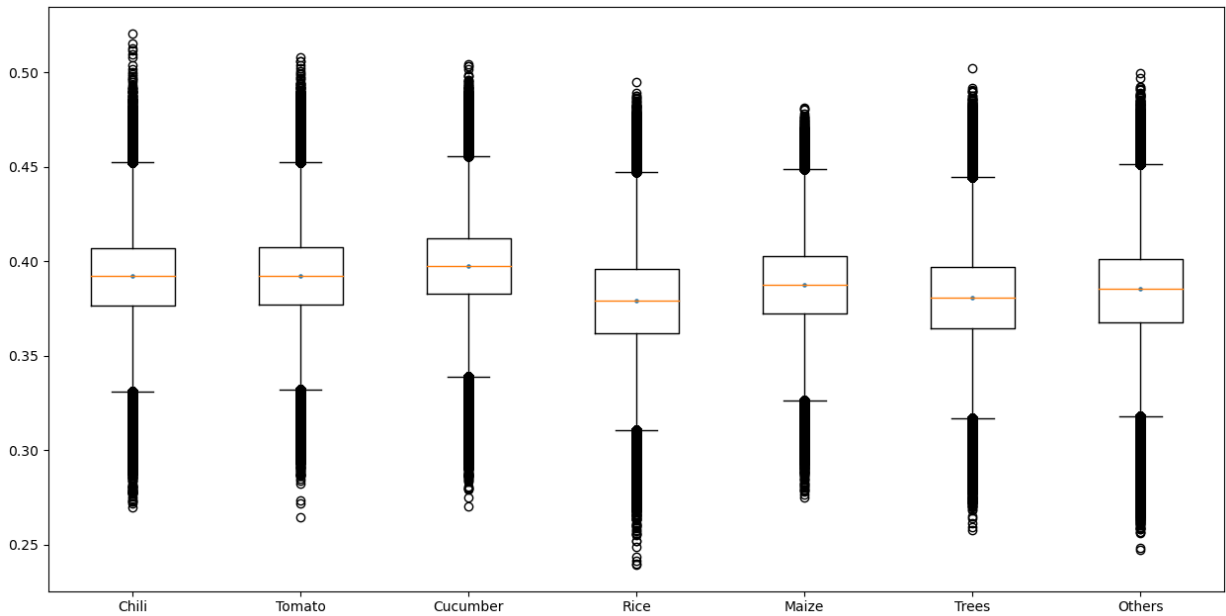


Figure 6: Distribution of the TWDTWS distances for each class query using Boxplots with mean and median represented inside each boxplot with a horizontal line and scatter point respectively. Each boxplot has a number of outliers.

4.4. Normalised fuzzy membership result

Spatial distribution of the normalised fuzzy membership to the best class for all the class queries is presented in Figure 7. These results show a unique pattern of the spatial distribution of the memberships. Figure 8 shows the normalised fuzzy membership for the runner-up class. The results shows that the spatial extent of the memberships to the runner-up class follow a similar pattern as the best class. The difference in spatial

patterns between best class and runner-up is that areas where best class recorded higher values the runner-up class has low values.

Areas with high memberships to the best class mostly belong to agriculture fields as can be seen from a subset of the Google Earth image in Figure 9(b). Figure 9(a) is a subset for the normalised fuzzy membership to the best class, whereas Figure 9(b) is the subset of the same area from Google Earth. The two subsets have clearly shown that even in agriculture fields there are also areas with low membership to the best class. The other thing is that the area has mountains dominated with tree cover, whereas agriculture is practiced in relatively flat terrain as presented in the subset of the Google Earth image.

4.5. Measures of similarity and uncertainty

4.5.1. Confusion Index

The spatial distribution of the computed CI based on the normalised fuzzy memberships is shown in Figure 10. The results show that CI ranges from 0.02 to 0.83. The areas where the CI values are low means that there is less confusion between the best class and the runner-up class. On the other hand, areas where the CI is high means the best class and runner class are similar hence high confusion.

4.5.2. Ambiguity Index

Spatial distribution of the computed AI from the normalised fuzzy membership to the best class and the best possible class membership ($\mu = 1$) is presented in Figure 11. The results show that areas where the AI is low means there is less uncertainty, while areas that have a higher AI correspond to high uncertainty. The range for the AI obtained is from 0.01 to 0.42.

4.5.3. Fuzziness Index

Spatial distribution of the computed fuzziness from the normalised fuzzy membership to the best class and runner-up class is presented in Figure 12. The results show that the range for the fuzziness values is from 0.04 to 1.67. The areas where fuzziness is high means that the pixels have membership values for the normalised best class and that of the normalised runner class closer to 0.5. On the other hand, areas, where the fuzziness is lower means that the normalised fuzzy memberships to the best class and the runner-up class are closer to 1 and 0, respectively.

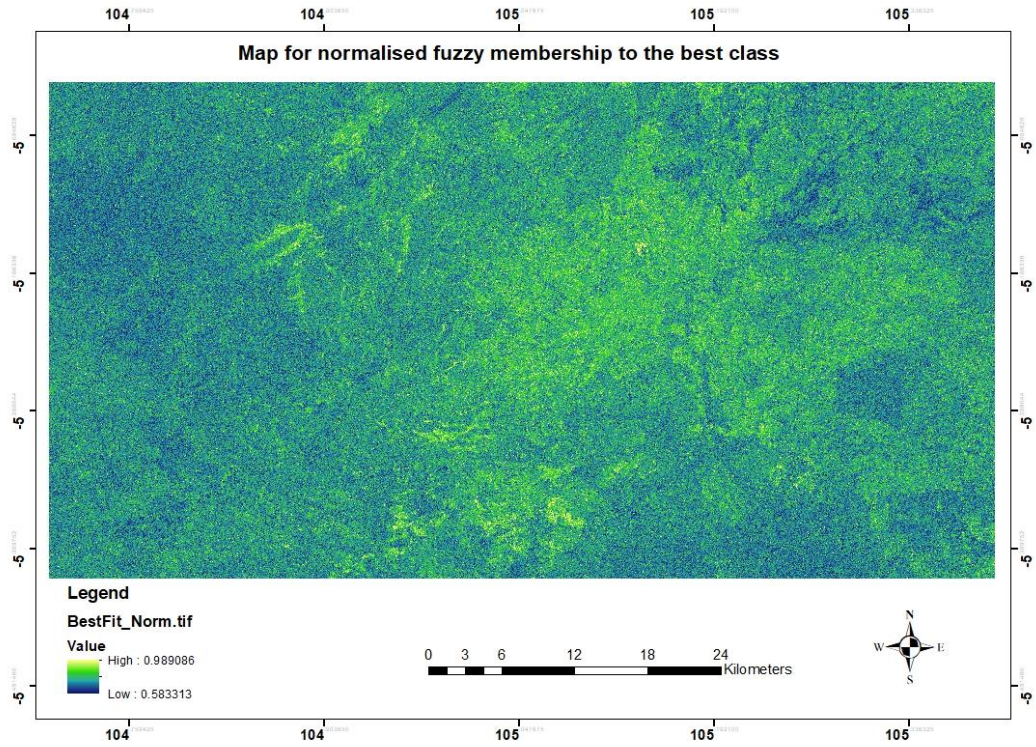


Figure 7: Spatial distribution for fuzzy membership to the normalised best class. The extent of fuzzy membership to the best class ranges from 0.58 to 0.99.

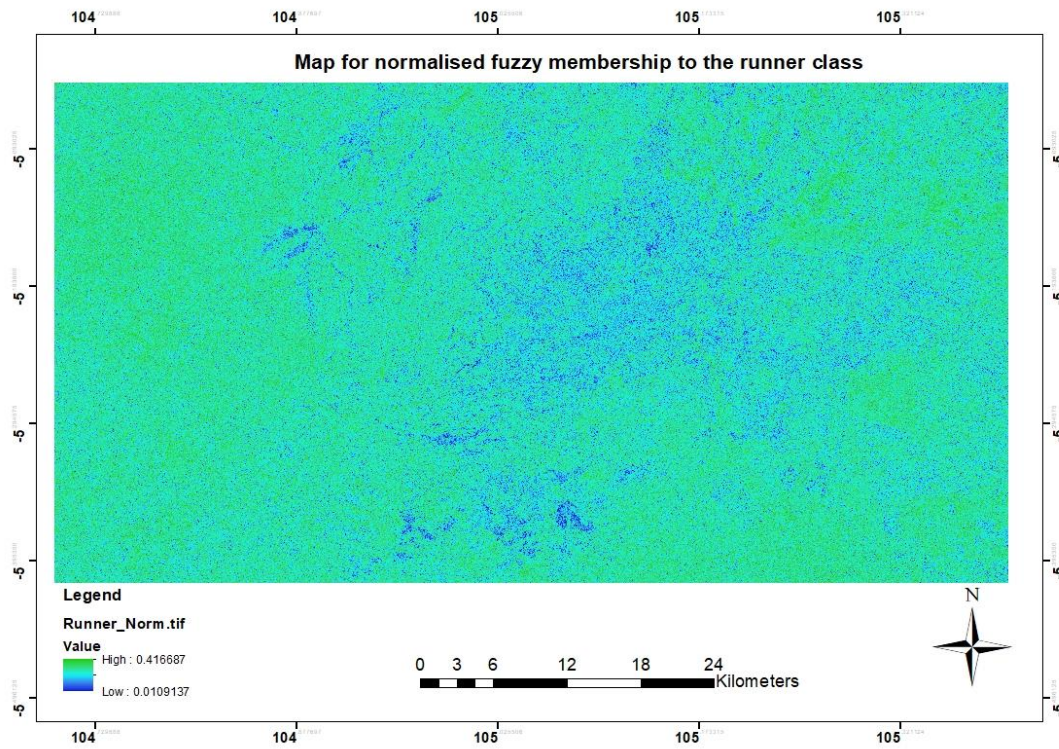
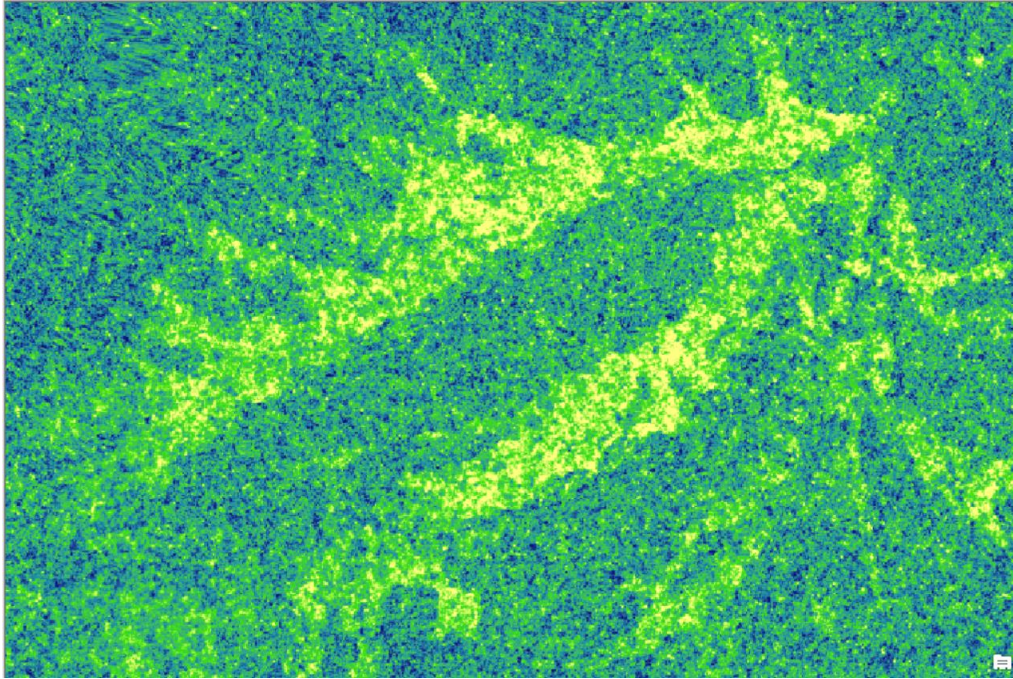


Figure 8: Spatial extents of the fuzzy membership for the normalised runner-up class. The extent of the fuzzy membership to the runner-up class ranges from 0.01 to 0.42.



(a)



(b)

Figure 9: (a) Subset of the study site for the normalised fuzzy membership to the best class; (b) Subset of the Google Earth image corresponding to the subset of Figure 9(a). The areas with high fuzzy membership correspond to an agricultural crop field, while areas with trees and mixed land cover type have low fuzzy membership, as can be seen from a Google Earth image. Dark blue means low fuzzy membership values, while yellow is high membership values. The area is composed of both mountain areas with and flat terrain where agriculture is practiced.

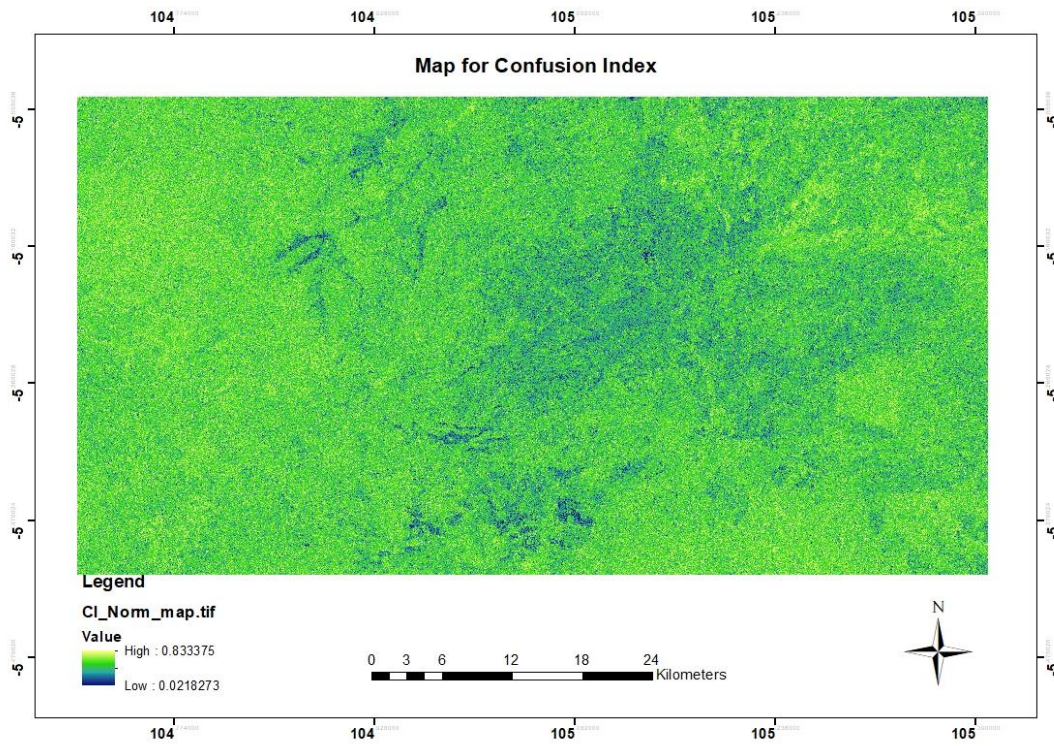


Figure 10: CI map showing the spatial distribution of CI. If areas have low CI, it means that similarity between the best class and runner-up class is not close, but in areas where CI is high, it means that the best class and the runner-up class are similar hence high confusion at the pixel level.

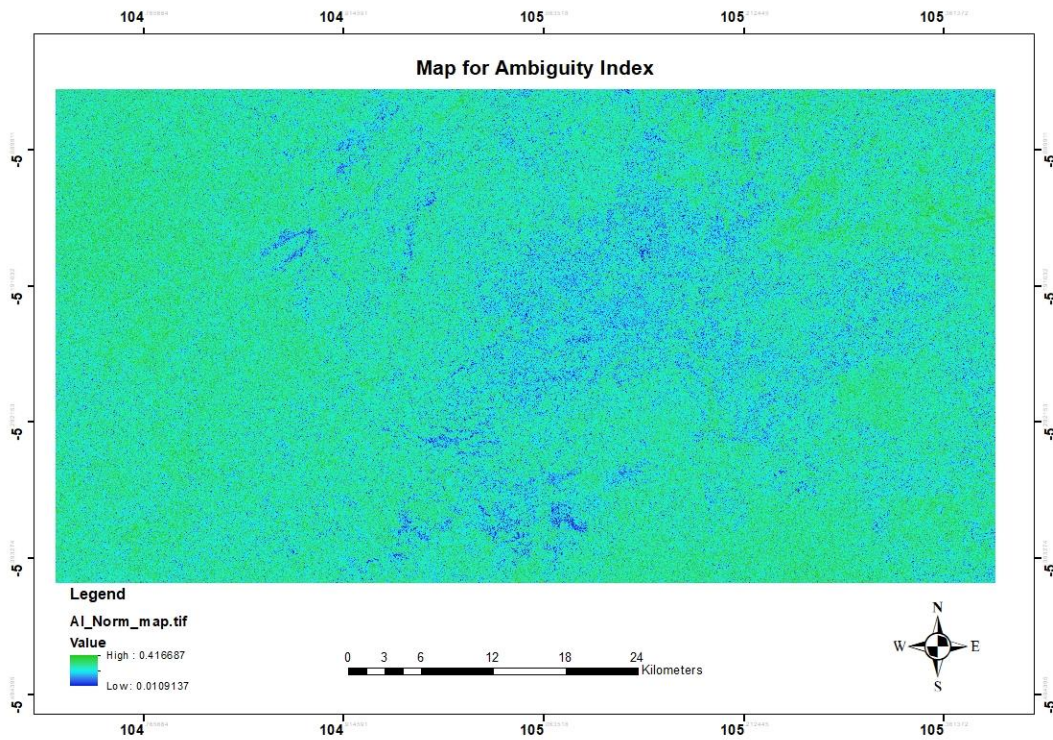


Figure 11: AI map showing the spatial distribution of AI. Areas where the AI is low means that there is less uncertainty between the best possible class and the best achieved class while areas where the AI is high means there is high uncertainty as the difference between the best possible class and the achieved best class is large.

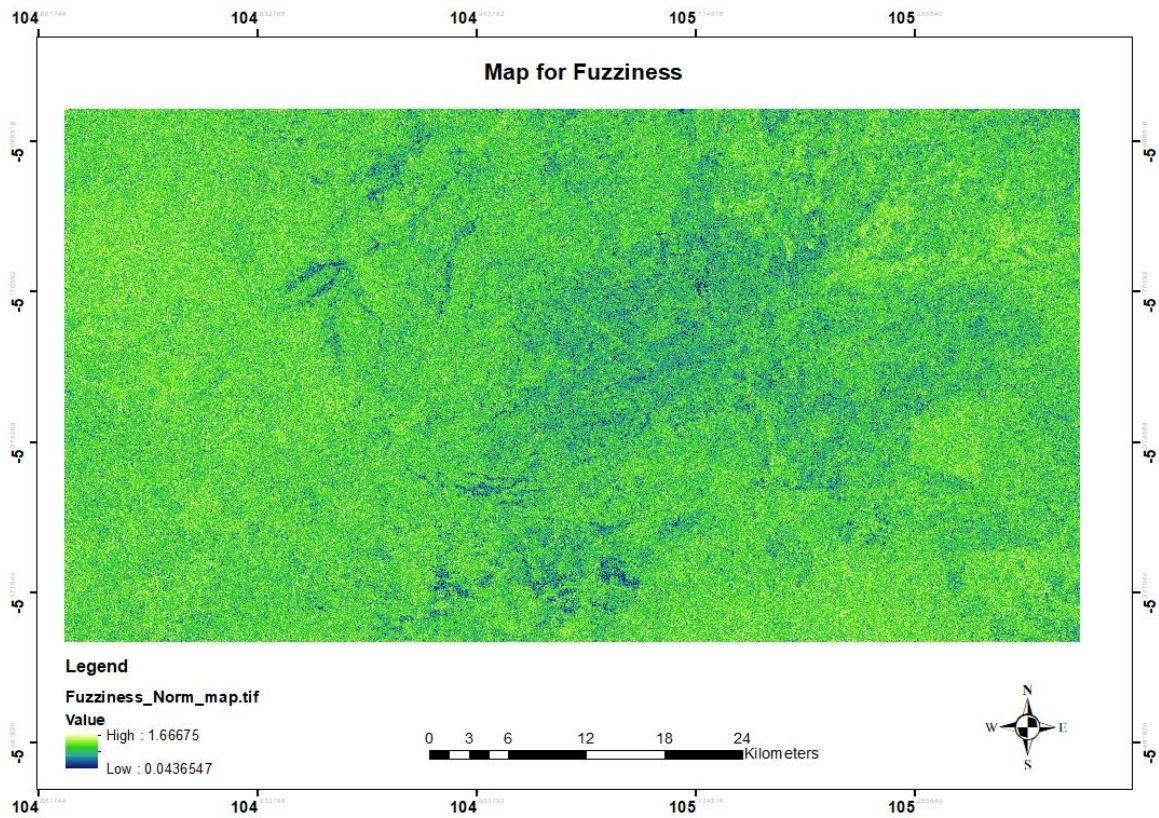


Figure 12: Fuzziness map showing the spatial distribution of the fuzziness for all the normalised fuzzy membership classes. High fuzziness means that those pixels have more fuzzy memberships closer to or equal to 0.5. If fuzziness is low, the pixels have fuzzy memberships closer to 1 and 0 for the best and runner-up class, respectively.

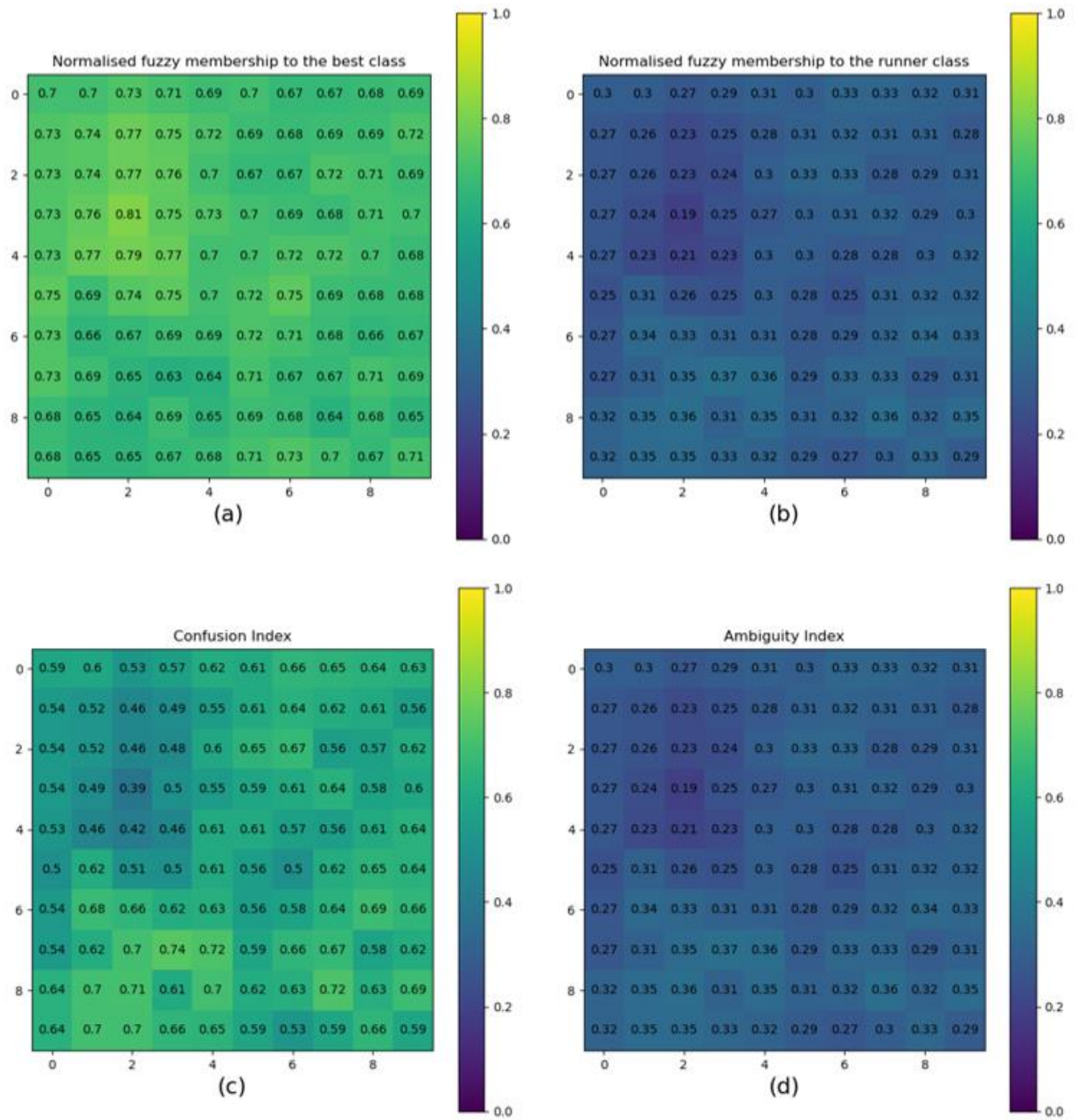


Figure 13: Subset of the study area the computation results for (a) Normalised fuzzy membership to the best class (b) Normalised fuzzy membership to the runner-up class (c) CI (d) AI. Pixels whose best class and runner-up class being similar have high CI while those that are not similar have low CI. Pixels with high values for the fuzzy membership to the best class have lower AI, while low values of best class results into high AI.

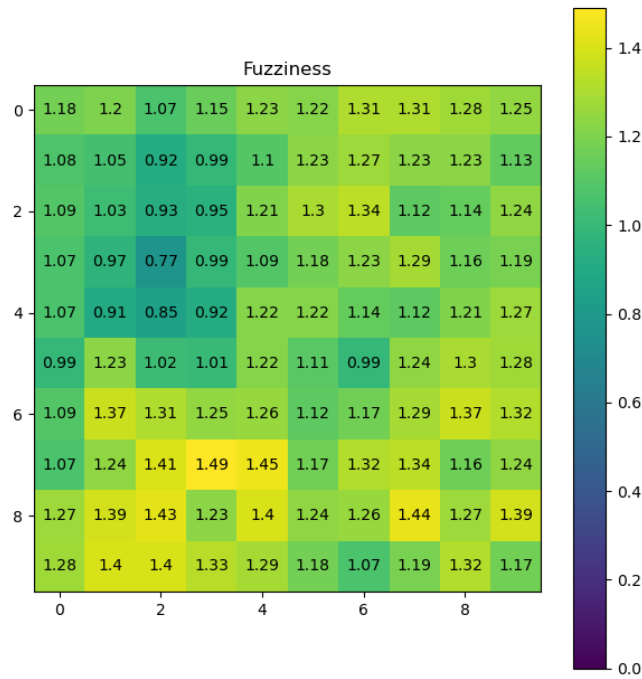


Figure 14: Subset of the study area showing the computational results for fuzziness. Pixels that have best class membership close to 1 and the runner-up class close to 0 have low fuzziness while those that have both membership classes closer to 0.5 have the highest values for fuzziness.

4.6. Defuzzification results

Table 6 shows the results for the percentage of pixels classified using different thresholds for CI, AI, fuzziness, and the normalised fuzzy membership to the best class. The results show that when $AI \leq 0.3$, 51.74% of pixels are classified. In the case of CI, when $CI \leq 0.6$, 51.74% of pixels are classified and 95.64% when the threshold for CI is $CI \leq 0.7$. A normalised fuzzy membership with threshold of $\mu \geq 0.7$ leads to 51.74% of the image pixels to be classified whereas fuzziness with thresholds of $Fuzz1 \leq 1.2$ and $Fuzz1 \leq 1.4$ has 51.74% and 95.64% of the pixels classified respectively. The number of classified pixels increases with increasing value for the threshold on AI, CI and fuzziness. In contrast to the normalised fuzzy membership, the number of pixels classified decreases with an increase in threshold value.

The spatial extent for the results for the defuzzification output for thresholds of $AI \leq 0.3$, $CI \leq 0.6$, $CI \leq 0.7$, $Fuzz1 \leq 1.2$, $Fuzz1 \leq 1.4$ and $\mu \geq 0.7$ are presented in Figure 15-20.

Figure 21 shows the subsets of some of the selected field samples used in this study area from Google Earth for comparison purpose as the time the Google Earth image was stored the field might have a different crop or no crop at all.

Table 6: Percentage of the total number of pixels classified based on the defuzzification threshold applied.

Threshold	% classified pixels (AI)	Threshold	% classified pixels (CI)	Threshold	% classified pixels (μ for best class)	Threshold	% classified pixels (Fuzziness)
AI \leq 0.1	0.01	CI \leq 0.1	0	$\mu \geq$ 0.1	100	Fuzz ₁ \leq 0.2	0
AI \leq 0.2	1.25	CI \leq 0.2	0.01	$\mu \geq$ 0.2	100	Fuzz ₁ \leq 0.4	0.01
AI \leq 0.3	51.74	CI \leq 0.3	0.1	$\mu \geq$ 0.3	100	Fuzz ₁ \leq 0.6	0.1
AI \leq 0.4	100	CI \leq 0.4	1.25	$\mu \geq$ 0.4	100	Fuzz ₁ \leq 0.8	1.25
AI \leq 0.5	100	CI \leq 0.5	11.03	$\mu \geq$ 0.5	100	Fuzz ₁ \leq 1.0	11.03
AI \leq 0.6	100	CI \leq 0.6	51.74	$\mu \geq$ 0.6	100	Fuzz ₁ \leq 1.2	51.74
AI \leq 0.7	100	CI \leq 0.7	95.64	$\mu \geq$ 0.7	51.74	Fuzz ₁ \leq 1.4	95.64
AI \leq 0.8	100	CI \leq 0.8	100	$\mu \geq$ 0.8	1.25	Fuzz ₁ \leq 1.6	100
AI \leq 0.9	100	CI \leq 0.9	100	$\mu \geq$ 0.9	0.01	Fuzz ₁ \leq 1.8	100

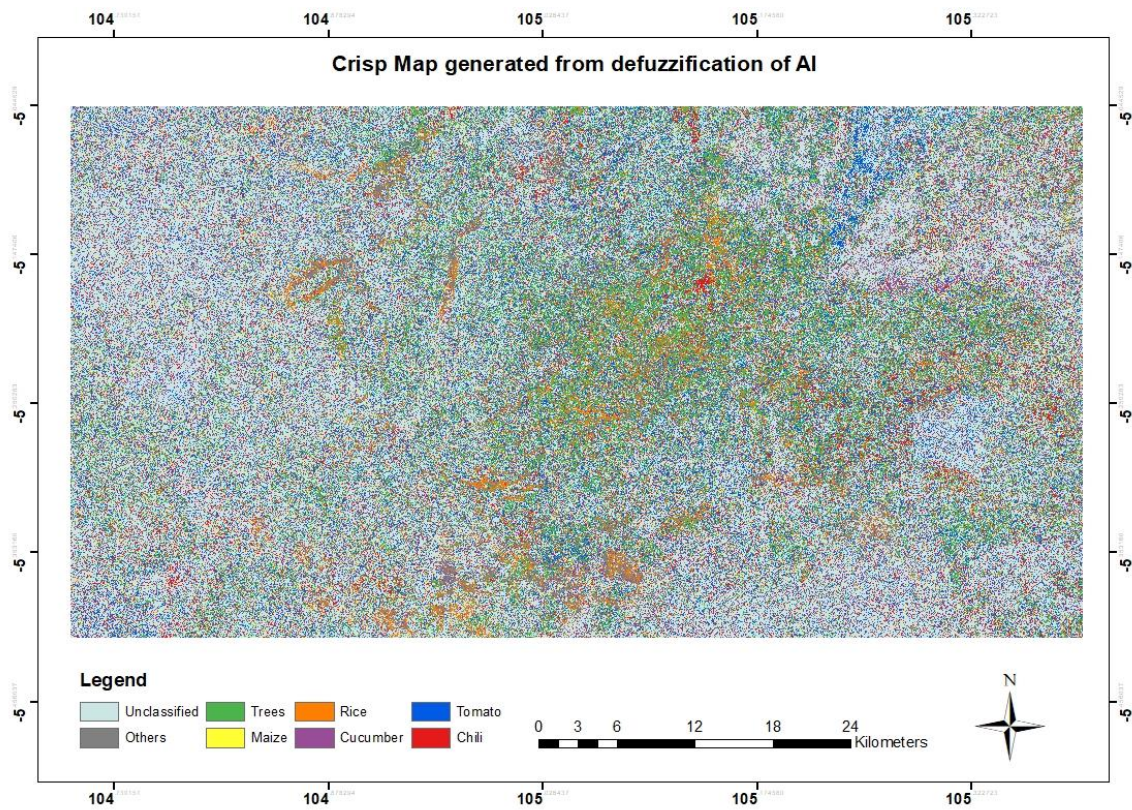


Figure 15: Crisp map generated from defuzzification of AI with a threshold of 0.3 where 51.74% pixels of the total image are classified.

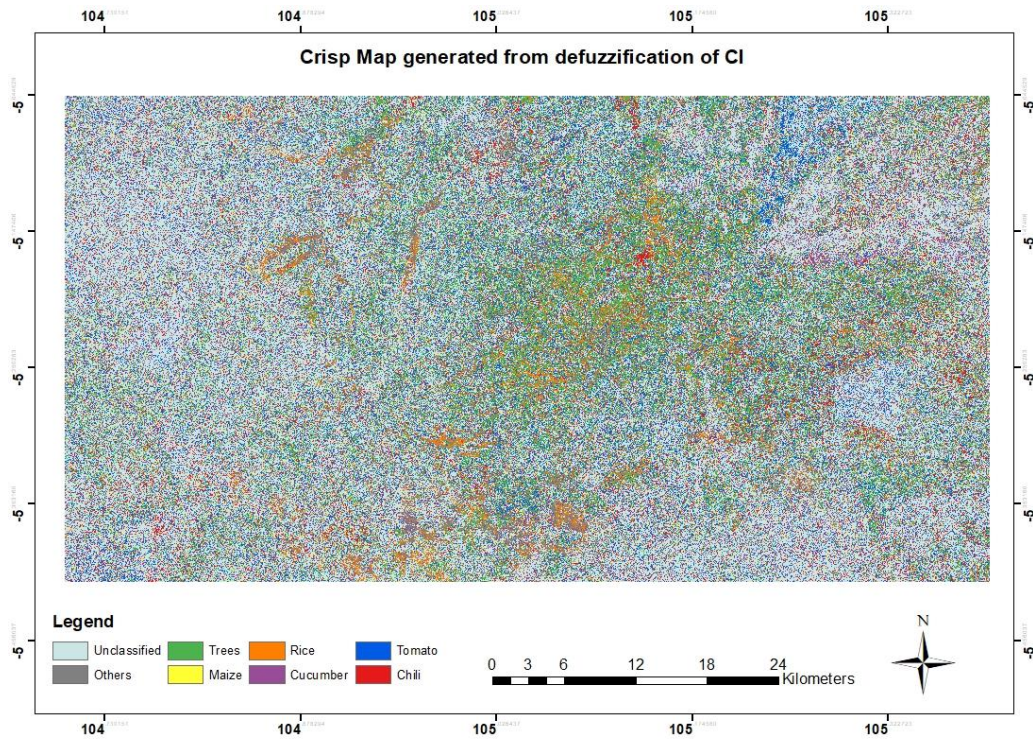


Figure 16: Crisp map generated from defuzzification of CI with a threshold of 0.6 where 51.74% pixels of the total image classified.

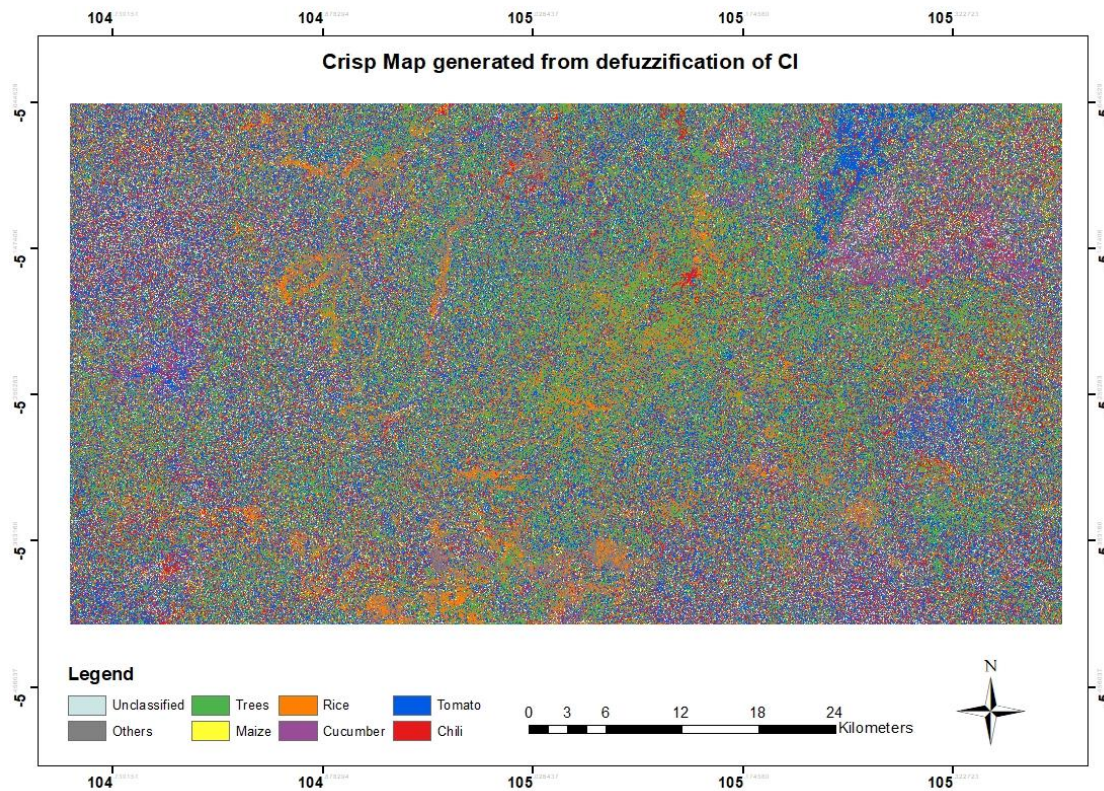


Figure 17: Crisp map generated from defuzzification of CI with a threshold of 0.7 where 95.64% pixels of the total image classified.

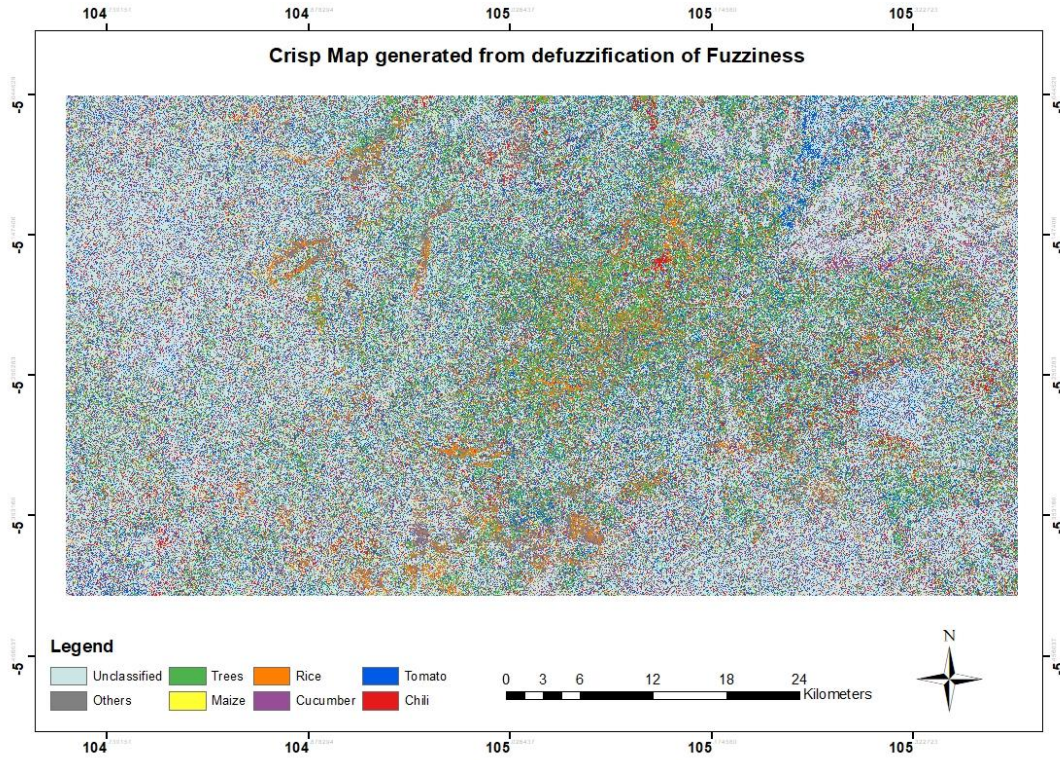


Figure 18: Crisp map generated from defuzzification of fuzziness with a threshold of 1.2 where 51.74% pixels of the total image classified.

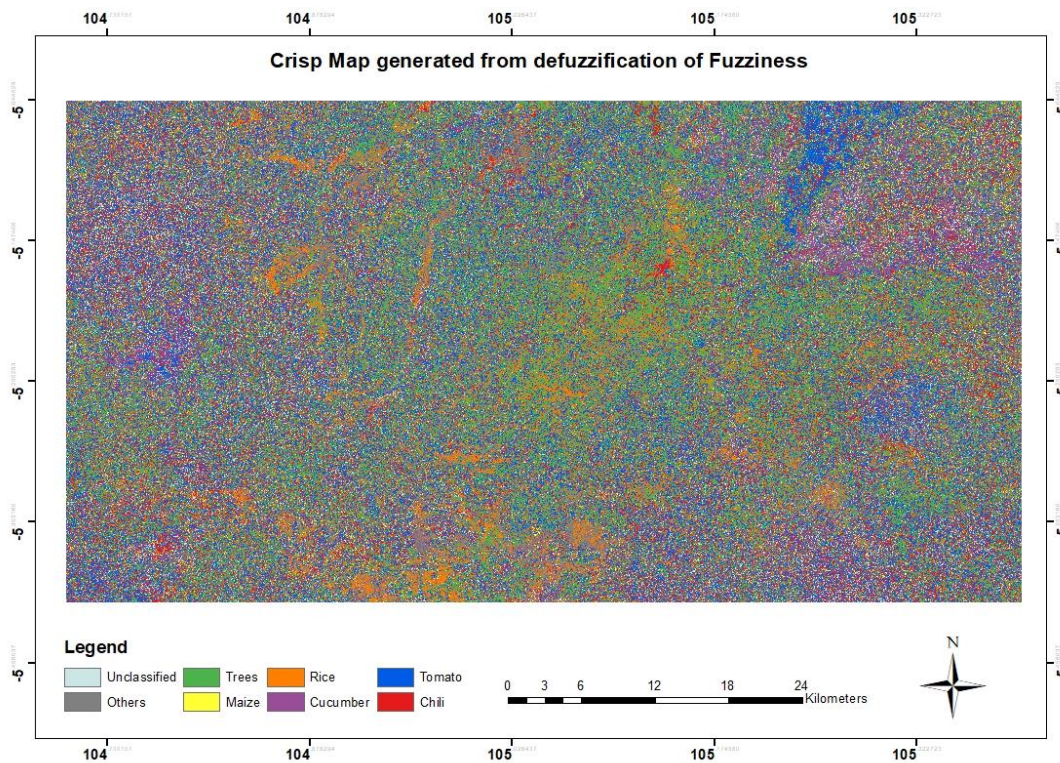


Figure 19: Crisp map generated from defuzzification of fuzziness with a threshold of 1.4, where 95.64% pixels of the total image classified.

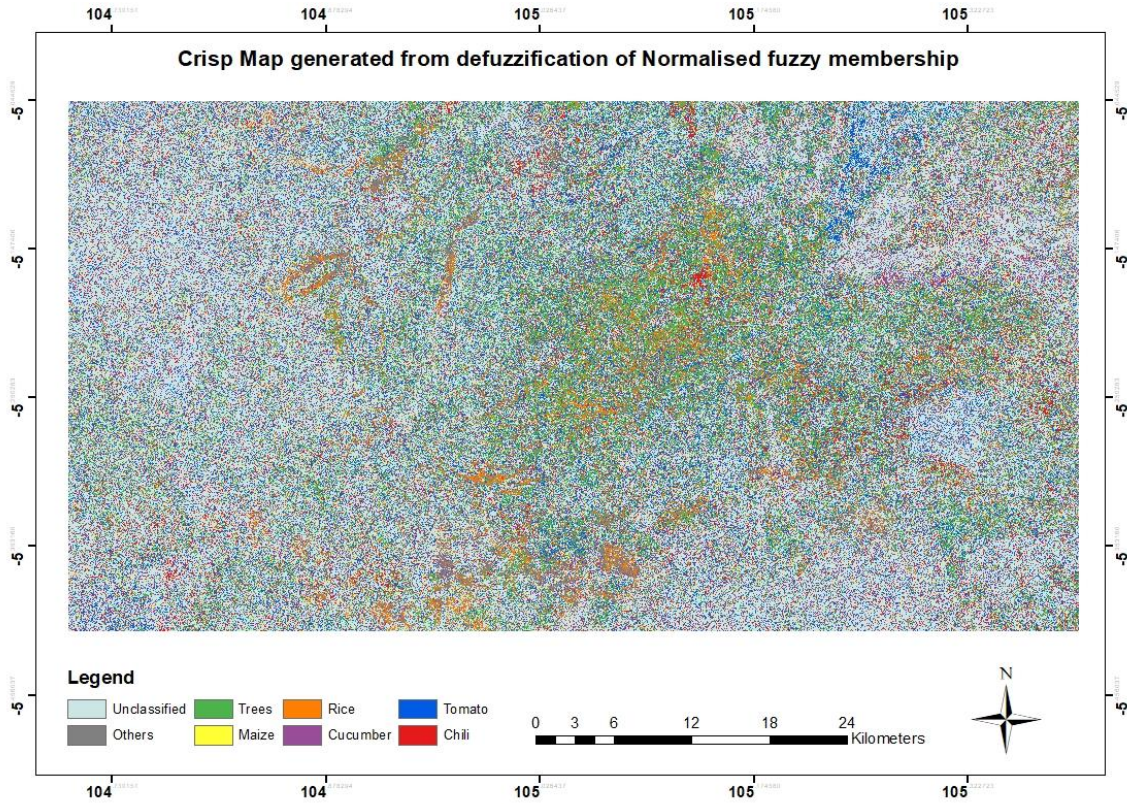


Figure 20: Crisp map generated from defuzzification of fuzzy membership with a threshold of 0.7, where 51.74% pixels of the total image classified.



Figure 21: Google Earth image subsets of the field study sites. (A) Chilli (B) Tomato (C) Cucumber (D) Rice (E) Maize (F) Trees and Others. It can be seen that the field study sample for Trees class has different cover classes.

4.7. Accuracy assessment

The overall accuracy and kappa coefficient in the research based on the defuzzification thresholds of $AI \leq 0.3$, $CI \leq 0.6$, $CI \leq 0.7$, $Fuzz_1 = 1.2$, $Fuzz_1 = 1.4$ and $\mu = 0.7$ is presented in Table 7. The overall accuracy for AI ($AI = 0.3$), CI ($CI = 0.6$), Fuzziness ($Fuzz_1 = 1.2$), Fuzziness ($Fuzz_1 = 1.4$) and fuzzy membership ($\mu = 0.7$) is 0.86, 0.86, 0.76, 0.86, 0.76 and 0.86 respectively. On the other hand, kappa coefficients are 0.83, 0.83, 0.72, 0.83, 0.72 and 0.83 on threshold AI ($AI = 0.3$), CI ($CI = 0.6$), Fuzziness ($Fuzz_1 = 1.2$), Fuzziness ($Fuzz_1 = 1.4$) and fuzzy membership ($\mu = 0.7$) respectively. The results for User's accuracy and Producer's accuracy is presented in Figures 22 and 23, respectively. The Error matrix for the accuracy assessment is in Tables 8-13 in the Appendix. The User's accuracy for thresholds AI ($AI = 0.3$), CI ($CI = 0.6$), Fuzziness ($Fuzz_1 = 1.2$) and fuzzy membership ($\mu = 0.7$) is relatively higher as compared to the User's accuracy for Fuzziness CI ($CI = 0.6$) and ($Fuzz_1 = 1.4$). The User's accuracy for all the classes for the thresholds chosen shows that the classes are well classified. However, in the Producer's accuracy, the classes for Maize and Trees have low results all the thresholds chosen. In each of the thresholds for $AI \leq 0.3$, $CI \leq 0.6$, $Fuzz_1 \leq 1.2$ and $\mu \geq 0.7$, the Producer's accuracy for Maize and Trees is 0.45 and 0.32 respectively. In the case of the thresholds of $CI \leq 0.7$ and $Fuzz_1 \leq 1.4$, the Producer's accuracy for Maize and Trees for each threshold are 0.47 and 0.47, respectively.

Table 7: Overall accuracy and Kappa coefficient of the defuzzification output for AI, CI, fuzziness, and fuzzy membership to the best class.

	Overall accuracy	Kappa coefficient
AI ($AI \leq 0.3$)	0.86	0.83
CI ($CI \leq 0.6$)	0.86	0.83
CI ($CI \leq 0.7$)	0.76	0.72
Fuzziness ($Fuzz_1 \leq 1.2$)	0.86	0.83
Fuzziness ($Fuzz_1 \leq 1.4$)	0.76	0.72
Fuzzy membership ($\mu \geq 0.7$)	0.86	0.83

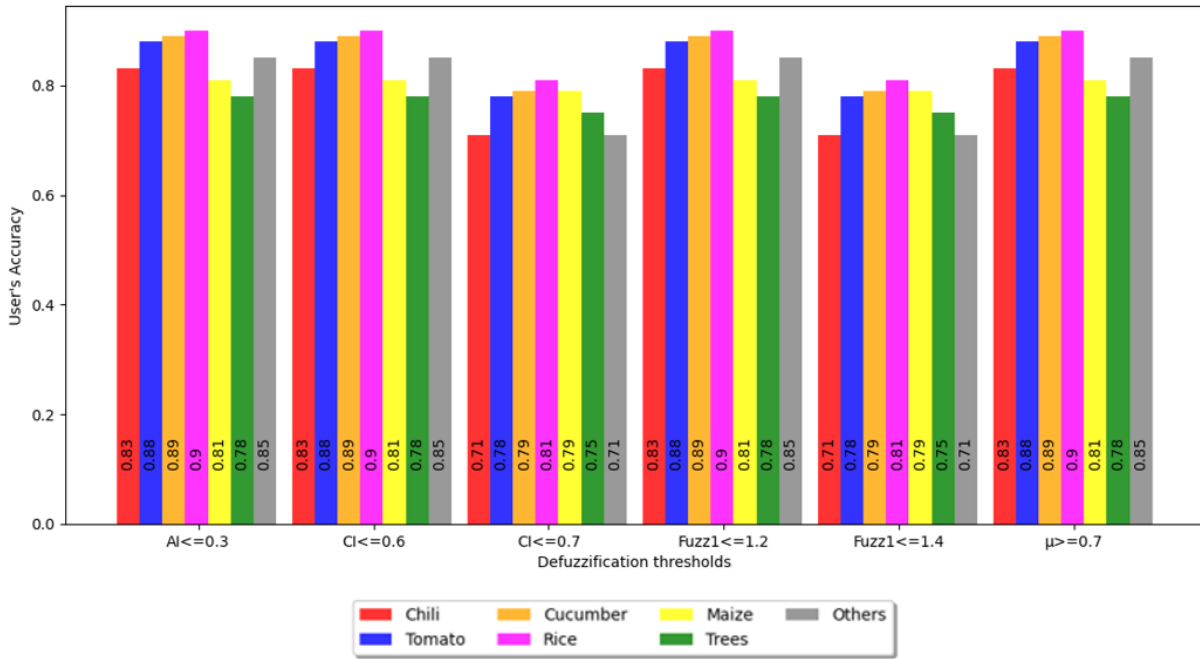


Figure 22: User's accuracy of the defuzzification outputs for AI , CI , $fuzziness$ and $fuzzy$ membership to the best class. $AI \leq 0.3$, $CI \leq 0.6$, $Fuzz1 = 1.2$ and $\mu \geq 0.7$ have higher and similar User's accuracy compared to $CI \leq 0.7$ and $Fuzz1 = 1.4$.

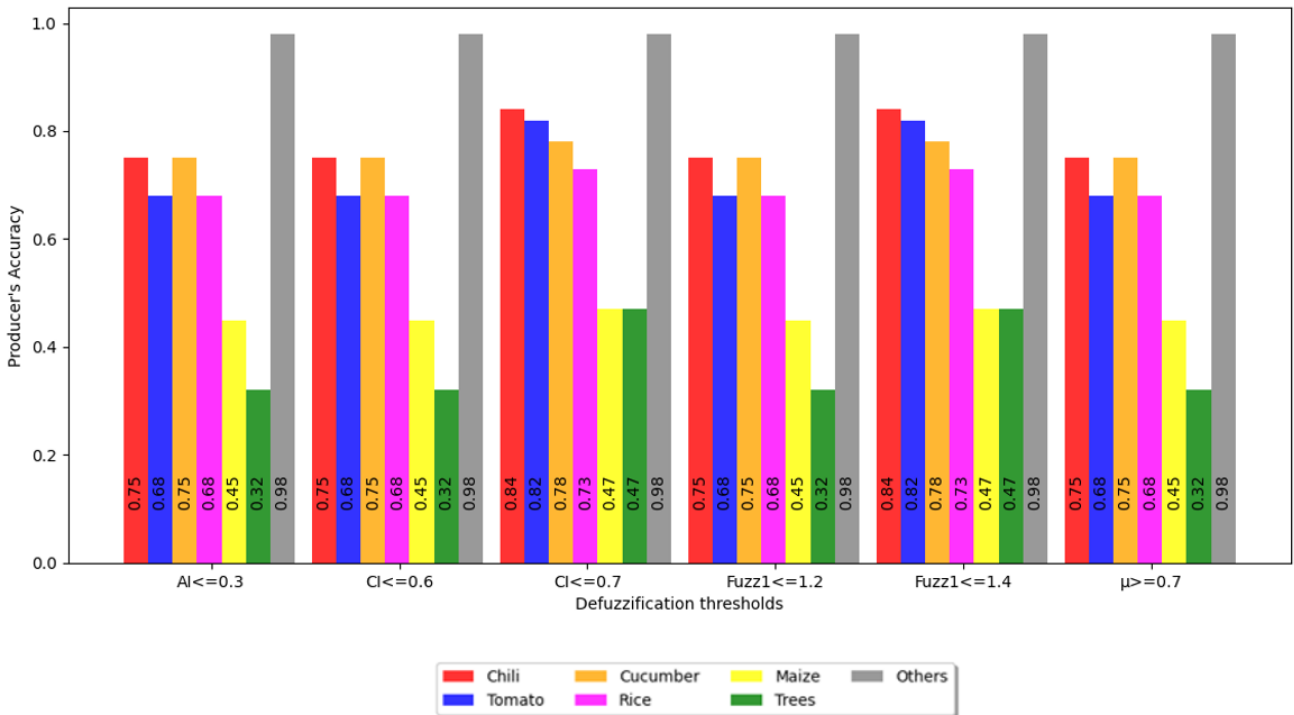


Figure 23: Producer's accuracy of the defuzzification outputs for AI , CI , $fuzziness$ and $fuzzy$ membership to the best class where $CI \leq 0.7$ and $Fuzz1 = 1.4$ have higher and similar Producer's accuracy compared to $AI \leq 0.3$, $CI \leq 0.6$, $Fuzz1 = 1.2$ and $\mu \geq 0.7$.

5. DISCUSSION

5.1. Class separability

The TD results in this study indicate that VH polarisation has better class separability as compared to VV and VH minus VV. Separability of vegetable pairs for Chili, Tomato and Cucumber using VH has higher TD values of 2000. This is similar to the class pair of Tomato-Trees, Cucumber-Trees and Rice-Trees with values of 2000 in the VH polarisation as presented in Table 2. When these pairs are compared to those obtained for VV and VH minus VV in Tables 3 and 4, respectively, the TD values obtained with VH are better. This is because values for TD equal to 2000, are considered to be excellent, while those below 1700 are poorly separable (Jensen, 2015). On the other hand, It has to be noted that based on the VH polarisation, the pair of Maize-Others shows smaller separability of 1713 just slightly above 1700. In the case of VV polarisation, the most the class pairs that are separable but slightly lower than those for the VH polarisation. The class pairs that are not separable using the VV polarisation include Chili-Maize, Tomato-Maize, Cucumber-maize, Rice-Maize, Tomato-Trees, Rice-Trees, Maize-Trees and Maize-Others. In the case of VH minus VH, the class pairs that are separable are Chili-Rice and Tomato-Rice, whereas the rest of the pair are not separable.

Furthermore, the growth pattern for the crops shows distinct patterns in terms of identifying the start and end of the season, more especially with VH polarisation. This is because in the VH polarisation, different target classes are better separable than the VV and VH minus VV as reviewed by the TD results. Based on the VH polarisation, the approximate lengths of the cropping cycles are Chili 96 days (DoY 145 to 241), Tomato 60 days (DoY 229 to 289), Cucumber 48 days (DoY 241 to 289), Rice 120 days (DoY 121 to 241) and Maize 72 days (DoY 145 to 217). These results are closely similar to those reported by Li & Bijker (2019).

5.2. TWDTWS distances

The results for the TWDTWS distances generated by the TWDTWS algorithm shows that they are normally distributed (slightly negatively skewed). The results for the boxplots of the TWDTWS distances show that there are outliers in the classified TWDTWS distance as shown in Figure 6. The outliers in the data consist of the excellent and relatively less good matches between the training query and the test query based on the distances. Excellent matches are the pixel whose TWDTWS distances are very small. The distribution of the TWDTWS distances is dependent on the quality of the training set used in the TWDTWS algorithm. Therefore, in order to achieve better results, the training data is a representation of the actual class proportions in the landscape (Millard & Richardson, 2015).

5.3. Spatial extent of CI, AI and fuzziness

The results from the study have shown that CI follows a unique pattern across the study as shown in Figure 10. Areas with low CI have are mostly covered by agricultural fields. The reason for low CI in the agriculture fields is because of the homogeneity of the crops in the pixels, which means that a single pixel in crop field has higher fuzzy membership to the best class than the runner-up class in a particular pixel (Burrough et al., 1997). In the case of Trees class, in most cases, there are gaps and also different landcover classes occurring in a pixel. The effect of the mixed pixel has a direct effect on the proportion of area each class the pixel will cover (Chhikara, 1984) when assigning fuzzy membership. This results into the fuzzy membership to the best class to be closely similar to the runner-up class (Hofmann, 2016). However, in the agriculture fields, some pixels show high CI and this could be due to various management practices and soil nutrients influencing the growth of the crop. Since the Radar signal is sensitive to soil moisture and water content in the canopy of vegetation, farm management practices such as irrigation can influence Radar backscattering at the time of image acquisition (Huang, Sun, Ni, Zhang, & Dubayah, 2015). This can occur when the field is not flat. This can later affect the TWDTWS classification during the generation of TWDTWS distances.

The spatial distribution for AI in this study has also revealed that it follows a unique pattern, just like CI as shown in Figure 11. The pattern shows that areas where CI has high values, AI also has higher values and vice versa. The reason for the high values of AI means that the pixels have a higher uncertainty (Hofmann, 2016). Similarly, the spatial pattern for fuzziness follows a unique pattern, just like CI and AI as presented in Figure 12. Higher values of fuzziness for some of the pixels is due to the pixels having memberships of 0.5 that are contributing to the uncertainty in these pixels from the crisp set (Siler & Buckley, 2004).

The spatial pattern for CI, AI and fuzziness have shown that close similarity in terms of the values obtained. These measures of similarity and uncertainty have in all cases, showing a similar spatial extent of the uncertainty. In most of the agriculture fields the values for AI, CI and fuzziness are low as compared to the trees class. This is because of the homogeneity in the crop fields as compared to the trees class where there are open spaces and mixed diversity of trees species in a pixel. The mixture of landcover classes in a pixel has an influence on the fuzzy memberships in the trees class. This is because, in a mixed pixel, there are mixed spectral responses consisting of the target and background reflectance (Chhikara, 1984). Ranson (2000) reported that radar backscatter in a vegetated area is a function of water content and its spatial distribution as determined by the canopy structure and the underlying surface conditions. Underlying conditions such as management practices of agriculture crops such as irrigation can influence the growth rate of crops in a field. This will eventually affect the fuzzy membership of the pixel due to the spectral variation from the crops in the pixel. The spectral variation from landcover types in a pixel affects the performance of the TWDTWS classifier in terms of the TWDTWS distance the pixel will have and the class label assigned to it. The variation of the spectral signature in pixel and that of the training set for the TWDTWS algorithm will affect the result of the fuzzy memberships the class will have.

Generally, the spatial pattern for CI, AI and fuzziness are similar in terms of where pixels have higher uncertainty. However, CI in this study is the preferred measure of uncertainty because it takes into account fuzzy membership to the best class and that of the runner-up class (Burrough et al., 1997). On the other hand, AI focusses solely on how the fuzzy membership of the achieved best class result differs from the possible best class result without taking into account the runner-up class. In the case of fuzziness, it uses both the fuzzy membership for the best class and the runners class though its aim is to highlight how fuzzy membership sets deviate from crisp sets.

5.4. Defuzzification and validation

Different defuzzification thresholds on based CI, AI, fuzziness and the normalised fuzzy membership to the best class were conducted in this study to determine the best threshold that would bring about improved accuracy assessment results. The best result for the overall accuracy and kappa coefficient in this study is 0.86 and 0.83, respectively as presented in Table 7. These results were recorded by each of the thresholds of $AI \leq 0.3$, $CI \leq 0.6$, $Fuzz_1 \leq 1.2$ and $\mu \geq 0.7$. On the other hand, $CI \leq 0.7$ and $Fuzz_1 \leq 1.4$ each have similar results for the overall accuracy and kappa coefficient of 0.76 and 0.72, respectively. The overall accuracy and kappa coefficient for 0.86 and 0.83, respectively, is higher than the overall accuracy and kappa coefficient of 0.76 and 0.72, respectively is because of some pixels that remained unclassified. The results with better results had more pixels that remained unclassified and this brought about improved accuracy. The pixels that remained unclassified are the have high uncertainty based on the defuzzification rules used in this study. These results also show that most of the unclassified pixels might have initially been assigned to a wrong class by the TWD-TWS algorithm, as observed for an increase in overall accuracy and kappa coefficient. It can be established that this approach of fuzzy classification on the TWD-TWS distances can be used to improve the classification accuracy as reported by Wang (1990). This is because fuzzy classification is able to adequately the problem of mixed pixel problem as compared to hard classification (Fisher & Pathirana, 1990).

The User's accuracy as presented in Figure 22 shows that the classes are well classified. The results in all the thresholds for the User's accuracy shows that the classes are well classified. This means that the results to the reliable as the map generated represents what is really on the ground (Story & Congalton, 1986).

The Producer's accuracy as presented in Figure 23, shows that the classes for Maize and Trees in all the thresholds are very low. The reason for these results could be that there is a lot of misclassification with other classes hence low Producer accuracy. Misclassification can be due to unknown factors such as soil fertility and management as is the case of Maize. For example, soil fertility and irrigation can affect the growth of the crops either positively or negatively and eventually affect the phenological structure of the crop, such as the leaves and the stalk. The differences caused by the growth rate can have an effect in terms of how the plant responds to Radar backscatter. In the case of Trees, factors like leaves, branches, trunk,

landcover type and open spaces can influence the interaction with Radar backscatter. The way the Maize and Trees respond to the Radar backscatter signal will affect the TWDTWS distances and class labels generated by the TWDTWS Algorithm due to mismatch. The mismatch could also be the reason that explains why there are many pixels from the class of Trees and Maize, which are unclassified and less correct classified pixels.

Finally, this study has shown different defuzzification thresholds of $AI \leq 0.3$, $CI \leq 0.6$, $F_{uzz_1} \leq 1.2$ and $\mu \geq 0.7$ give similar results of overall accuracy, kappa coefficient, User's accuracy and Producer accuracy. Similarly, $CI \leq 0.7$ and $F_{uzz_1} \leq 1.4$ give similar results. Better overall accuracy, kappa coefficient and User's accuracy is better when there are many unclassified pixels. The benefit of having more unclassified pixels is that the pixels that have been misclassified and have high uncertainty will remain unclassified, thereby improving the classification accuracy. However, a trade-off between the classified and unclassified pixels should support the user in balancing between the crisp classification reliability and the amount of classified pixels covered in the study area (Hofmann, 2016). This means that a better number of pixels should be classified that can give better overall accuracy, kappa coefficient and User's accuracy so that the defuzzification product could be given confidence.

6. CONCLUSION AND RECOMMENDATIONS

6.1. Conclusion

This research presented fuzzy classification using TWD'TWS distances obtained from the TWD'TWS algorithm on Sentinel 1A images. The fuzzification of the minimum TWD'TWS distances was performed using the Gaussian membership function. The results of TD have shown that classes are better separable when using VH as compared to VV and VH minus VV.

The approach that was applied in this study has shown that accuracy assessment can be improved by using thresholds of $AI=0.3$, $CI=0.6$, $Fuzz1 = 1.2$ and $\mu = 0.7$. This is because of the high overall accuracy, kappa coefficient and producer accuracy that gives confidence and reliability of the classification process. The overall accuracy and kappa obtained in this study is 0.86 and 0.83, respectively, when 48.26% of the pixel for the study area remain unclassified. On the other hand, when 4.36% of the pixels remain unclassified, the overall accuracy and kappa coefficient is 0.76 and 0.72, respectively. The results get improved because pixels that were initially assigned to wrong classes by the TWD'TWS algorithm are unclassified, thereby improving the accuracy. The pixels with high uncertainty are unclassified thereby ensuring that only pixels with better fuzzy membership as stipulated by the users are to be classified.

Finally, this study has shown that AI, CI, fuzziness and fuzzy membership to the best class can be used in fuzzy classification to provide a better result when a careful selection of defuzzification thresholds is applied. However, defuzzification using CI is a preferred method based on the fact that it focusses on the similarities between the best class and runner-up class to compute similarities as compared to AI, fuzziness and fuzzy membership to the best class.

6.2. Recommendation

Based on the finding of this research, further work should be undertaken in assessing the quality of training and validation samples in remote sensing so that locations that have a high certainty of best class fuzzy membership of the information class are selected.

LIST OF REFERENCES

- Banuwa, I. S., Afriliyanti, R., Utomo, M., Yusnaini, S., Riniarti, M., Sanjaya, P., ... Hidayat, W. (2019). Short communication: Estimation of the above-and below-ground carbon stocks in university of lampung, Indonesia. *Biodiversitas*, 20(3), 676–681. <https://doi.org/10.13057/biodiv/d200309>
- Bezdek, James C., Robert Ehrlich, & William Full. (1984). FCM: The Fuzzy C-Means Clustering Algorithm. *Computers and Geosciences*, 10(2), 191–203.
- Bezdek, J. C., Ehrlich, R., & Full, W. (1984). FCM: The Fuzzy c-Means Clustering Algorithm. *Computers and Geosciences*, 10(2), 191–203. <https://doi.org/10.1109/igarss.1988.569600>
- Burrough, P. A., Van Gaans, P. F. M., & Hootsmans, R. (1997). Continuous classification in soil survey: Spatial correlation, confusion and boundaries. *Geoderma*, 77(2–4), 115–135. [https://doi.org/10.1016/S0016-7061\(97\)00018-9](https://doi.org/10.1016/S0016-7061(97)00018-9)
- Chang-an, L., Zhong-xin, C., Yun, S., Jin-song, C., Hasi, T., & Hai-zhu, P. (2019). Research advances of SAR remote sensing for agriculture applications: A review. *Journal of Integrative Agriculture*, 18(3), 506–525. [https://doi.org/10.1016/S2095-3119\(18\)62016-7](https://doi.org/10.1016/S2095-3119(18)62016-7)
- Chhikara, R. S. (1984). Effect of mixed (boundary) pixels on crop proportion estimation. *Remote Sensing of Environment*, 14(1–3), 207–218. [https://doi.org/10.1016/0034-4257\(84\)90016-6](https://doi.org/10.1016/0034-4257(84)90016-6)
- Choodarathnakara, A. L., Ashok Kumar, T., Koliwad, S., & Patil, C. G. (2012). Soft Classification Techniques for RS Data. *International Journal of Computer Science Engineering and Technology (IJCSET)*, 2(11), 1468–1471. Retrieved from <http://ijcset.net/docs/Volumes/volume2issue11/ijcset2012021101.pdf>
- Congalton, R. G. (1991). A review of assessing the accuracy of classifications of remotely sensed data. *Remote Sensing of Environment*, 37(1), 35–46. [https://doi.org/10.1016/0034-4257\(91\)90048-B](https://doi.org/10.1016/0034-4257(91)90048-B)
- Dewi, N. K., Sasmito, A., Aziz, I. R., Parwito, & Sari, K. N. (2019). Seagrass community at tawang coast pacitan in rainy and dry season. *Journal of Physics: Conference Series*, 1175(1). <https://doi.org/10.1088/1742-6596/1175/1/012007>
- Dusseux, P., Corpetti, T., Hubert-Moy, L., & Corgne, S. (2014). Combined use of multi-temporal optical and Radar satellite images for grassland monitoring. *Remote Sensing*, 6(7), 6163–6182. <https://doi.org/10.3390/rs6076163>
- Fisher, P. F., & Pathirana, S. (1990). The evaluation of fuzzy membership of land cover classes in the suburban zone. *Remote Sensing of Environment*, 34(2), 121–132. [https://doi.org/10.1016/0034-4257\(90\)90103-S](https://doi.org/10.1016/0034-4257(90)90103-S)
- Foody, G. M. (1996). Approaches for the production and evaluation of fuzzy land cover classifications from remotely-sensed data. *International Journal of Remote Sensing*, 17(7), 1317–1340. <https://doi.org/10.1080/01431169608948706>
- Guan, X., Huang, C., Liu, G., Meng, X., & Liu, Q. (2016). Mapping rice cropping systems in Vietnam using an NDVI-based time-series similarity measurement based on DTW distance. *Remote Sensing*, 8(1). <https://doi.org/10.3390/rs8010019>
- Guan, X., Liu, G., Huang, C., Meng, X., Liu, Q., Wu, C., ... Wang, Q. (2018). An Open-Boundary Locally Weighted Dynamic Time Warping Method for Cropland Mapping. *ISPRS International Journal of Geo-Information*, 7(2), 75. <https://doi.org/10.3390/ijgi7020075>
- Hara, Y., McPhearson, T., Sampei, Y., & McGrath, B. (2018). Assessing urban agriculture potential: a comparative study of Osaka, Japan, and New York City, United States. *Sustainability Science*, 13(4), 937–952. <https://doi.org/10.1007/s11625-018-0535-8>
- Hofmann, P. (2016). Defuzzification strategies for fuzzy classifications of remote sensing data. *Remote Sensing*, 8(6). <https://doi.org/10.3390/rs8060467>
- Huang, W., Sun, G., Ni, W., Zhang, Z., & Dubayah, R. (2015). Sensitivity of multi-source SAR backscatter to changes in forest aboveground biomass. *Remote Sensing*, 7(8), 9587–9609. <https://doi.org/10.3390/rs70809587>
- Ibrahim, A., & Valli, C. (2015). Image similarity using dynamic time warping of fractal features. *13th Australian Digital Forensics Conference, 2015*, 111–122. <https://doi.org/10.4225/75/57b3fe44fb890>
- Islam, Z., & Metternicht, G. (2005). The performance of fuzzy operators on fuzzy classification of urban land covers. *Photogrammetric Engineering and Remote Sensing*, 71(1), 59–68. <https://doi.org/10.14358/PERS.71.1.59>
- Jensen, J. R. (2015). *Introductory Digital Image Processing: A remote sensing perspective* (4th Editio, Vol. 3). Pearson Education, Inc. Retrieved from <http://repositorio.unan.edu.ni/2986/1/5624.pdf>

- Jeong, Y. S., Jeong, M. K., & Omitaomu, O. A. (2011). Weighted dynamic time warping for time series classification. *Pattern Recognition*, *44*(9), 2231–2240. <https://doi.org/10.1016/j.patcog.2010.09.022>
- Jiang, H., Li, D., Jing, W., Xu, J., Huang, J., Yang, J., & Chen, S. (2019). Early Season Mapping of Sugarcane by Applying Machine Learning Algorithms to Sentinel-1A/2 Time Series Data: A Case Study in Zhanjiang City, China. *Remote Sensing*, *11*(7), 861. <https://doi.org/10.3390/rs11070861>
- Joosten, F., Dijkxhoorn, Y., Sertse, Y., & Ruben, R. (2015). How does the Fruit and Vegetable Sector contribute to Food and Nutrition Security? (p. 62). Wageningen: LEI Wageningen UR (University & Research centre), LEI Nota 2015-076.
- Klir, G. J., & Yuan, B. (1995). *Fuzzy sets and fuzzy logic: Theory and applications*. *Neurocomputing* (Vol. 14). New Jersey: Prentice Hall PTR. [https://doi.org/10.1016/s0925-2312\(97\)88327-0](https://doi.org/10.1016/s0925-2312(97)88327-0)
- Kumar, S., Saravana, G., Rout, R., Pandit, A., & Snehamani. (2012). Fuzzy-Based Sub-Pixel Classification of Satellite Imagery. *International Journal of Computer Science and Technology*, *3*(1), 593–598.
- Lee, J., Fellow, L., Ainsworth, T. L., Wang, Y., & Chen, K. (2015). Polarimetric SAR Speckle Filtering and the Extended Sigma Filter, *53*(3), 1150–1160.
- Li, L., Kong, Q., Wang, P., Xun, L., Wang, L., Xu, L., & Zhao, Z. (2019). Precise identification of maize in the North China Plain based on Sentinel-1A SAR time series data. *International Journal of Remote Sensing*, *40*(5–6), 1996–2013. <https://doi.org/10.1080/01431161.2018.1504345>
- Li, M., & Bijker, W. (2019). Vegetable classification in Indonesia using Dynamic Time Warping of Sentinel-1A dual polarization SAR time series. *International Journal of Applied Earth Observation and Geoinformation*, *78*(February), 268–280. <https://doi.org/10.1016/j.jag.2019.01.009>
- Liu, Y., Zhang, H. H., & Wu, Y. (2011). Hard or soft classification? large-margin unified machines. *Journal of the American Statistical Association*, *106*(493), 166–177. <https://doi.org/10.1198/jasa.2011.tm10319>
- Matsakis, P., Andréfouët, S., & Capolsini, P. (2000). Evaluation of fuzzy partitions. *Remote Sensing of Environment*, *74*(3), 516–533. [https://doi.org/10.1016/S0034-4257\(00\)00143-7](https://doi.org/10.1016/S0034-4257(00)00143-7)
- Maus, V., Camara, G., Cartaxo, R., Sanchez, A., Ramos, F. M., & de Queiroz, G. R. (2016). A Time-Weighted Dynamic Time Warping Method for Land-Use and Land-Cover Mapping. *IEEE Journal of Selected Topics in Applied Earth Observations and Remote Sensing*, *9*(8), 3729–3739. <https://doi.org/10.1109/JSTARS.2016.2517118>
- Millard, K., & Richardson, M. (2015). On the importance of training data sample selection in Random Forest image classification: A case study in peatland ecosystem mapping. *Remote Sensing*, *7*(7), 8489–8515. <https://doi.org/10.3390/rs70708489>
- Mosleh, M. K., Hassan, Q. K., & Chowdhury, E. H. (2015). Application of remote sensors in mapping rice area and forecasting its production: A review. *Sensors (Switzerland)*, *15*(1), 769–791. <https://doi.org/10.3390/s150100769>
- Najafi, A., Hasanlou, M., & Akbari, V. (2019). Change detection using distance-based algorithms between synthetic aperture radar polarimetric decompositions. *International Journal of Remote Sensing*, *40*(15), 6084–6097. <https://doi.org/10.1080/01431161.2019.1587202>
- Niennattrakul, V., & Ratanamahatana, C. A. (2007). On clustering multimedia time series data using k-means and dynamic time warping. *Proceedings - 2007 International Conference on Multimedia and Ubiquitous Engineering, MUE 2007*, 733–738. <https://doi.org/10.1109/MUE.2007.165>
- Onashoga, A., Ojesanmi, O., Johnson, F., & Ayo, F. E. (2018). A fuzzy-based decision support system for soil selection in olericulture. *Journal of Agricultural Informatics*, *9*(3). <https://doi.org/10.17700/jai.2018.9.3.480>
- Onojeghuo, A. O., Blackburn, G. A., Wang, Q., Atkinson, P. M., Kindred, D., & Miao, Y. (2018). Mapping paddy rice fields by applying machine learning algorithms to multi-temporal Sentinel-1A and Landsat data. *International Journal of Remote Sensing*, *39*(4), 1042–1067. <https://doi.org/10.1080/01431161.2017.1395969>
- Ranson, K. J. (2000). Effects of environmental conditions on boreal forest classification and biomass estimates with SAR. *IEEE Transactions on Geoscience and Remote Sensing*, *38*(3), 1242–1252. <https://doi.org/10.1109/36.843016>
- Sakoe, H., & Chiba, S. (1978). Dynamic Programming Algorithm Optimization for Spoken Word Recognition. *IEEE Transactions on Acoustics, Speech, and Signal Processing*, *26*(1), 43–49. <https://doi.org/10.1109/TASSP.1978.1163055>
- Sakurai, Y., Faloutsos, C., & Yamamuro, M. (2007). Stream monitoring under the time warping distance. *Proceedings - International Conference on Data Engineering*, 1046–1055. <https://doi.org/10.1109/ICDE.2007.368963>
- Savitzky, A., & Golay, M. J. E. (1964). Smoothing and Differentiation of Data by Simplified Least Squares

- Procedures. *Analytical Chemistry*, 36(8), 1627–1639. <https://doi.org/10.1021/ac60214a047>
- Schreinemachers, P., Simmons, E. B., & Wopereis, M. C. S. (2018). Tapping the economic and nutritional power of vegetables. *Global Food Security*, 16(September 2017), 36–45. <https://doi.org/10.1016/j.gfs.2017.09.005>
- Siler, W., & Buckley, J. J. (2004). *Fuzzy Expert Systems and Fuzzy Reasoning*. *Fuzzy Expert Systems and Fuzzy Reasoning*. New Jersey: John Wiley & Sons Ltd. <https://doi.org/10.1002/0471698504>
- Sitanggang, I. S., Agmalaro, M. A., Hendrik, & Li, M. (2019). *Automation of Image Processing Workflow as part of the Geodata for Agriculture and Water (G4AW) project “SMARTSeeds”, (SARauto report)*.
- Skolnik, M. i. (1990). *Radar Handbook*. McGraw-Hill (2nd Editio, Vol. 53). Boston: McGraw-Hill.
- SMARTSeeds. (2019). Information services for vegetable farmers in Indonesia (SMARTseeds). Retrieved September 18, 2019, from <http://smartseeds-indonesia.org/resources-materials/>
- SNAP. (2019). Sentinel Application Platform. Retrieved November 28, 2019, from <http://step.esa.int/main/toolboxes/snap/>
- Stendardi, L., Karlsen, S. R., Niedrist, G., Gerdol, R., Zebisch, M., Rossi, M., & Notarnicola, C. (2019). Exploiting time series of Sentinel-1 and Sentinel-2 imagery to detect meadow phenology in mountain regions. *Remote Sensing*, 11(5), 1–24. <https://doi.org/10.3390/rs11050542>
- Story, M., & Congalton, R. G. (1986). Remote Sensing Brief Accuracy Assessment: A User’s Perspective. *Photogrammetric Engineering and Remote Sensing*, 52(3), 397–399.
- Swain, P. H., & Davis, S. M. (Eds.). (1978). *Remote Sensing: The Quantitative Approach*. New York: McGraw-Hill.
- Switonski, A., Josinski, H., & Wojciechowski, K. (2018). Dynamic time warping in classification and selection of motion capture data. *Multidimensional Systems and Signal Processing*. <https://doi.org/10.1007/s11045-018-0611-3>
- Thenkabail, P. S. (2015). *Remotely sensed data characterization, classification, and accuracies*. (P. S. Thenkabail, Ed.), *Remotely Sensed Data Characterization, Classification, and Accuracies* (Volume 1, Vol. 1). New York, USA: Taylor & Francis Group, LLC. <https://doi.org/10.1201/b19294>
- Viana, C. M., Girão, I., & Rocha, J. (2019). Long-Term Satellite Image Time-Series for Land Use/Land Cover Change Detection Using Refined Open Source Data in a Rural Region. *Remote Sensing*, 11(9), 1104. <https://doi.org/10.3390/rs11091104>
- Wang, F. (1990). Fuzzy Supervised Classification of Remote Sensing Images. *IEEE Transactions on Geoscience and Remote Sensing*, 28(2), 194–201. <https://doi.org/10.1109/36.46698>
- Yang, Y., Wang, Y., Wu, K., & Yu, X. (2016). Classification of complex urban fringe land cover using evidential reasoning based on fuzzy rough set: A case study of Wuhan City. *Remote Sensing*, 8(4), 1–17. <https://doi.org/10.3390/rs8040304>

7. APPENDIX

Table 8: Error matrix for a crisp map of CI with a threshold of 0.6.

		Chili	Tomato	Cucumber	Rice	Maize	Trees	Others	Unclassified	Row Total	Producer's Accuracy
Reference	Chili	70	1	0	4	1	3	1	13	80	0.75
	Tomato	3	76	0	0	0	4	0	28	83	0.68
	Cucumber	2	0	76	0	4	0	0	19	82	0.75
	Rice	1	1	2	66	1	3	7	16	81	0.68
	Maize	4	0	4	1	26	0	1	22	36	0.45
	Trees	4	8	3	1	0	35	2	56	53	0.32
	Others	0	0	0	1	0	0	63	0	64	0.98
	Column Total	84	86	85	73	32	45	74		479	
	User's Accuracy	0.83	0.88	0.89	0.90	0.81	0.78	0.85			
	Overall Accuracy										
Kappa											0.83

Table 9: Error matrix for a crisp map of CI with a threshold of 0.7.

		Chili	Tomato	Cucumber	Rice	Maize	Trees	Others	Unclassified	Row Total	Producer's Accuracy
Reference	Chili	78	1	0	7	1	4	1	1	92	0.84
	Tomato	6	91	5	0	0	7	0	2	109	0.82
	Cucumber	8	0	79	0	4	1	1	8	93	0.78
	Rice	3	2	3	71	1	3	9	5	92	0.73
	Maize	4	4	8	3	27	2	5	5	53	0.47
	Trees	11	19	5	6	1	51	10	6	103	0.47
	Others	0	0	0	1	0	0	63	0	64	0.98
	Column Total	110	117	100	88	34	68	89		606	
	User's Accuracy	0.71	0.78	0.79	0.81	0.79	0.75	0.71			
	Overall Accuracy										
Kappa											0.72

Table 10: Error matrix for a crisp map of AI with a threshold of 0.3.

		Chili	Tomato	Cucumber	Rice	Maize	Trees	Others	Unclassified	Row Total	Producer's Accuracy
Reference	Chili	70	1	0	4	1	3	1	13	80	0.75
	Tomato	3	76	0	0	0	4	0	28	83	0.68
	Cucumber	2	0	76	0	4	0	0	19	82	0.75
	Rice	1	1	2	66	1	3	7	16	81	0.68
	Maize	4	0	4	1	26	0	1	22	36	0.45
	Trees	4	8	3	1	0	35	2	56	53	0.32
	Others	0	0	0	1	0	0	63	0	64	0.98
	Column Total	84	86	85	73	32	45	74		479	
	User's Accuracy	0.83	0.88	0.89	0.90	0.81	0.78	0.85			
	Overall Accuracy										
Kappa											0.83

Table 11: Error matrix for a crisp map of fuzziness with a threshold of 1.2.

		Chili	Tomato	Cucumber	Rice	Maize	Trees	Others	Unclassified	Row Total	Producer's Accuracy
Reference	Chili	70	1	0	4	1	3	1	13	80	0.75
	Tomato	3	76	0	0	0	4	0	28	83	0.68
	Cucumber	2	0	76	0	4	0	0	19	82	0.75
	Rice	1	1	2	66	1	3	7	16	81	0.68
	Maize	4	0	4	1	26	0	1	22	36	0.45
	Trees	4	8	3	1	0	35	2	56	53	0.32
	Others	0	0	0	1	0	0	63	0	64	0.98
	Column Total	84	86	85	73	32	45	74		479	
	User's Accuracy	0.83	0.88	0.89	0.90	0.81	0.78	0.85			
	Overall Accuracy										
Kappa											0.83

Table 12: Error matrix for a crisp map of fuzziness with a threshold of 1.4.

		Chili	Tomato	Cucumber	Rice	Maize	Trees	Others	Unclassified	Row Total	Producer's Accuracy
Reference	Chili	78	1	0	7	1	4	1	1	92	0.84
	Tomato	6	91	5	0	0	7	0	2	109	0.82
	Cucumber	8	0	79	0	4	1	1	8	93	0.78
	Rice	3	2	3	71	1	3	9	5	92	0.73
	Maize	4	4	8	3	27	2	5	5	53	0.47
	Trees	11	19	5	6	1	51	10	6	103	0.47
	Others	0	0	0	1	0	0	63	0	64	0.98
	Column Total	110	117	100	88	34	68	89		606	
	User's Accuracy	0.71	0.78	0.79	0.81	0.79	0.75	0.71			
	Overall Accuracy										
Kappa											0.72

Table 13: Error matrix for a crisp map of normalised fuzzy membership for best class with a threshold of 0.7.

		Chili	Tomato	Cucumber	Rice	Maize	Trees	Others	Unclassified	Row Total	Producer's Accuracy
Reference	Chili	70	1	0	4	1	3	1	13	80	0.75
	Tomato	3	76	0	0	0	4	0	28	83	0.68
	Cucumber	2	0	76	0	4	0	0	19	82	0.75
	Rice	1	1	2	66	1	3	7	16	81	0.68
	Maize	4	0	4	1	26	0	1	22	36	0.45
	Trees	4	8	3	1	0	35	2	56	53	0.32
	Others	0	0	0	1	0	0	63	0	64	0.98
	Column Total	84	86	85	73	32	45	74		479	
	User's Accuracy	0.83	0.88	0.89	0.90	0.81	0.78	0.85			
	Overall Accuracy										
Kappa											0.83